Melt mixing and crystallization under Theistareykir, northeast Iceland

J. Maclennan, D. Mckenzie, K. Grönvold, N. Shimizu, J. M. Eiler, N. Kitchen

HAL Id: insu-03598407

https://insu.hal.science/insu-03598407

Submitted on 6 Mar 2022

Melt mixing and crystallization under Theistareykir, northeast Iceland

J. Maclennan

Bullard Laboratories, Department of Earth Sciences, Madingley Road, Cambridge, CB3 0EZ, UK

Now at Laboratoire de Géosciences Marines, Institut de Physique du Globe de Paris, France (maclenna@ipgp.jussieu.fr)

D. McKenzie

Bullard Laboratories, Department of Earth Sciences, Madingley Road, Cambridge, CB3 0EZ, UK
(mckenzie@esc.cam.ac.uk)

K. Grönvold

Nordic Volcanological Institute, Reykjavik, Iceland (karl@norvol.hi.is)

N. Shimizu

Department of Geology and Geophysics, Woods Hole Oceanographic Institution, Woods Hole, Massachusetts 02543, USA
(nshimizu@whoi.edu)

J. M. Eiler and N. Kitchen

Division of Geological and Planetary Sciences, California Institute of Technology, Pasadena, California 91125, USA
(eiler@gps.caltech.edu)

[1] Analysis of the compositions of crystals and melt inclusions from a suite of 40 gabbroic and wehrlitic nodules in a single eruptive body provides a record of concurrent mixing and crystallization of melts under NE Iceland. The crystals in the nodules have a similar range of compositions to those found as phenocrysts in the flow, and many of the nodules may have been generated by crystallization of a magma with a similar composition to that of the host flow. While plagioclase is only present in nodules where the average forsterite content of olivines is $<Fo_{88.5}$, clinopyroxene is found in nodules with average olivine forsterite contents of up to $Fo_{91.6}$. The order of crystallization $ol \rightarrow ol + cpx \rightarrow ol + cpx + plg$ is consistent with generation of the nodules at pressures >0.8 GPa and is in agreement with estimates of crystallization pressures for the host basalt. The relationship between the compositional variability of melt inclusions and the forsterite content of the host olivine is revealed by REE analyses of over 120 melt inclusions. The degree of variability in REE concentrations and REE/Yb ratios decreases with falling forsterite content of the host olivine, as expected if melt mixing and fractional crystallization are operating together. The standard deviation of the REEs falls by a factor of $\sim$4 between Fo_{90} and Fo_{87}. This change in olivine composition can be produced by crystallization of 20% which occurs on cooling of $\sim$50°C. The relative rates of mixing, cooling and crystallization may provide constraints upon the dynamics of magma bodies. The oxygen isotopic composition of olivines from the nodules and phenocrysts is highly variable ($\delta^{18}O$ from $3.3-5.2$ per mil) and shows little correlation with the forsterite content of the olivine. The full range of oxygen isotope variation is present in olivines with Fo_{89-90}, and the low $\delta^{18}O$ signal is associated with melts of high Mg# and La/Yb. Such geochemical relationships cannot be produced by assimilation of low Mg# crustal materials alone, and may reflect oxygen isotopic variation within the mantle source. The geochemistry of the melt inclusions and their host crystals can be accounted for by fractional melting of a mantle source with variable composition, followed by concurrent mixing and crystallization beneath the Moho.

————————————————

Theme: The Oman Ophiolite and Mid-Ocean Ridge Processes
Guest Editors: Peter Kelemen, Chris MacLeod, and Susumu Umino

1. Introduction

[2] The last twenty years have seen the assembly of a compelling set of geochemical, geophysical and experimental evidence that indicates that mantle melting beneath mid-ocean ridges is near-fractional [*Kelemen et al.*, 1997]. Melts that are generated by decompression during mantle upwelling separate from the solid mantle residue at small porosities and rapidly ascend toward the surface in isolated conduits. The compositions of melts generated during progressive fractional melting vary with the depth and extent of melting and a large range of instantaneous melt compositions are generated over the depth interval of melting. This variability is most apparent for incompatible trace elements, such as the light Rare Earth Elements (REEs). Melts generated at the onset of melting near the base of the melting region have light REE concentrations that are tens of times higher than those of the mantle source. After a few percent of melting the light REEs are stripped from the mantle residue, and any further melting of this residue during decompression will generate fractional melts with light REE concentrations approaching zero. If the composition of mantle entering the melting region is variable, then the available spread of melt compositions will be enlarged. The range of melt compositions predicted by progressive fractional melting of even a single source is far greater than that found in basalts at mid-ocean ridges. Therefore fractional melts must be extensively mixed prior to their eruption. Little is known about the depth or physical environment where mixing takes place, or about the rate of mixing with respect to other processes. The composition of the mantle melts is related to those of mid-ocean ridge basalt (MORB) samples by mixing, so understanding of the mixing process is required for interpretation of MORB compositions in terms of the bulk properties of large volumes of mantle.

[3] Iceland is an excellent place to study mixing of mantle melts because it is straightforward to collect large numbers of samples from eruptions of well-constrained age and volume from its active volcanic zones. The Theistareykir segment of the Northern Volcanic Zone of Iceland has been particularly well studied, and geochemical variability has been identified within whole-rock samples and olivine-hosted melt inclusions from a number of young (<12 kyr BP), primitive eruptions. The presence of this variability shows that melts cannot have been perfectly mixed and allows detailed study of the mixing process to be undertaken. The Theistareykir whole-rock samples have variable major and trace element and radiogenic isotope compositions [*Elliott et al.*, 1991; *Slater et al.*, 2001; *Stracke et al.*, 2003] and oxygen isotope variability is also present in crystals within these eruptions [*Eiler et al.*, 2000]. This variability is also found within single eruptions and the Borgarhraun flow has been the target of detailed study [*Maclennan et al.*, 2003; *Stracke et al.*, 2003; *Eiler et al.*, 2000]. While the presence of trace element and radiogenic isotope variability within Theistareykir has been shown to result from variations in mantle melt compositions [*Elliott et al.*,

1991; *Slater et al.*, 2001; *Maclennan et al.*, 2002; *Stracke et al.*, 2003], the oxygen isotope variability has been attributed to crustal processes [*Eiler et al.*, 2000]. Melt inclusions hosted by olivine and chromian spinel phenocrysts from Borgarhraun have compositions that are far more variable than those of the host lava [*Sigurdsson et al.*, 2000; *Maclennan et al.*, 2003], indicating that extensive mixing took place after the onset of crystallization.

[4] The aim of the present study is to constrain the location and extent of mixing and crystallization of mantle melts under Theistareykir. New measurements of the major and trace element and oxygen isotope composition of crystals from a suite of wehrlitic and gabbroic nodules from Borgarhraun are presented, along with new REE data from 35 olivine-hosted melt inclusions and 38 points from clinopyroxenes. The major element composition and modal mineralogy of the nodules are used to estimate the depth of crystallization and mixing. A relationship between the REE variability of the melt inclusions and the forsterite content of the host olivines is observed and used to quantify relative rates of melt mixing, crystallization and cooling of melt under Theistareykir. Such estimates may provide constraints on physical models of magma bodies under spreading ridges. The origin of the oxygen isotope variation in Borgarhraun olivines is then investigated by relating the $\delta^{18}O$ of crystals to their major and trace element composition and the REE composition of the melt inclusions that they host. The data are not consistent with supply of a single primary melt composition from the mantle followed by closed system fractional crystallization in the crust, and indicate that interpretation of MORB data-sets in terms of a liquid line of descent from a primary melt must be undertaken with caution. Instead, the compositions of the melt inclusions and crystals hosted by the Borgarhraun flow can be accounted for by fractional melting of a heterogeneous mantle source followed by concurrent mixing and crystallization near the Moho under Theistareykir.

2. Sample Collection and Preparation

[5] Borgarhraun is one of a number of primitive lava shields that erupted in Theistareykir during early postglacial times (12–7 kyr BP). The Borgarhraun lava was erupted from a crater near its eastern limit and then flowed westward into the main graben of the Theistareykir system in a number of discrete flow events. The north-south and east-west extents of Borgarhraun are both ~10 km and its total surface area is ~35 km². The spatial distribution of compositional variation within Borgarhraun was described by *Maclennan et al.* [2003]. Rock samples containing ~50 polycrystalline nodules of >1 cm diameter were collected from the Borgarhraun lava flow during July 1999. All of the nodules were collected from within 100 m of 65°51.05′N, 16°59.93′N which is the location of a small depression at the eastern edge of the flow. Inspection of the hand-specimens showed that most of the nodules were gabbros, with a limited number of wehrlites, troctolites and dunites also present. The largest nodule was approximately 5 cm in diameter. The nodule margins are sharp and there is little macroscopic evidence for chemical reaction between the nodules and their host lava. Along with the nodules, the samples contain olivine, clinopyroxene and plagioclase phenocrysts [*Maclennan et al.*, 2003]. The samples were cleaned and sections of 35 of the nodules were prepared for petrographic and electron probe compositional analyses. Crystals were hand picked from a number of the nodules for trace element and oxygen isotope analyses.

2.1. Petrography

[6] The nodules display a wide range of textures in thin section, with poikilitic wehrlites and ophitic to granular gabbros and troctolites (Figure 1). The nodules do not appear to have undergone extensive brittle or plastic deformation and only one of the gabbros (JM29n1) contains plagioclase with tapering lamellar twins. The nodules are extremely fresh and show little evidence of alteration or growth of hydrous phases. There is also little evidence of extensive reaction between the nodules and their host magmas, although a number of olivines at the edges of nodules appear to have narrow rims (<20 μm) with lower forsterite content than the core. A number of the nodules appear to be disaggregating within the host basalt. Approximate modal mineralogies of the nodules were estimated using point counting, and the results of this point counting
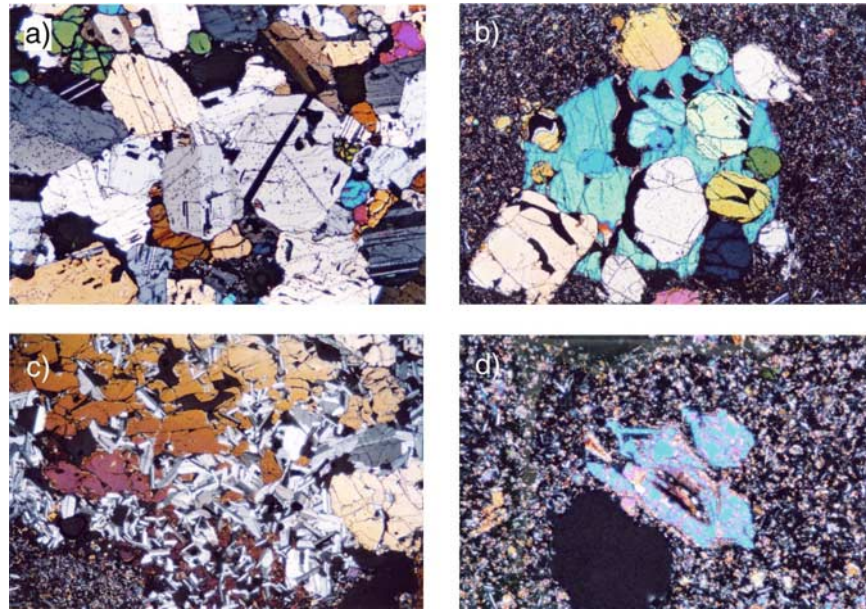
Figure 1. Thin sections of Borgarhraun nodules and phenocrysts viewed in cross-polarized light. (a) Anhedral granular troctolite JM18n1. Field of view is 6 mm. (b) Poikilitic wehrlite with olivine chadacrysts and a clinopyroxene oikocryst in JM03n1. Field of view is 6 mm. (c) Subophitic gabbro JM06. Field of view is 6 mm. (d) Skeletal olivine phenocryst in sample JM11. Field of view is 3 mm.

are given in Table 1. The nodules do not exhibit any coherent layered structure, which may result from their limited size.

[7] The phenocryst population is dominated by olivine, with smaller proportions of clinopyroxene and plagioclase. Point counting analysis of the Borgarhraun thin sections has shown that by volume the phenocryst population is composed of 87% olivine, 7% plagioclase, 6% clinopyroxene and 0.4% Mg-Al-chromite [*Maclennan et al.*, 2003]. Several types of olivine phenocryst morphologies are present in the flow including euhedral, blocky and skeletal.

2.2. Compositional Analyses

2.2.1. Secondary Ionisation Mass Spectrometry

[8] The rare earth element (REE) composition of olivine-hosted melt inclusions and clinopyroxene crystals from the Borgarhraun nodules were measured using secondary ionization mass spectrometry (SIMS). Melt inclusions are common within olivines from the nodules. These inclusions appear to be primary magmatic inclusions and are often partly crystalline, similar to inclusions hosted in pheno-

cryst olivines from Borgarhraun [*Maclennan et al.*, 2003]. The melt inclusions were rehomogenized by heating in a vertical one atmosphere quench furnace held at 1240°C and an oxygen fugacity one log unit beneath the quartz-fayalite-magnetite buffer. The samples were held at these conditions for about 20 minutes in a Pt crucible and were quenched rapidly by dropping the crucible into water. Next, the crystals were set in epoxy and the melt inclusions were exposed by grinding and polishing with Buehler Alpha diamond and alumina micropolish. Inspection of the melt inclusions after heating showed that they were glassy, devoid of bubbles and had recovered their preheating shape. The Cameca IMS 3f ion probe at Woods Hole Oceanographic Institute was used to analyse 35 melt inclusions from 24 olivines from 10 nodules and 38 points in 26 clinopyroxenes from 9 nodules for selected REE concentrations. The compositions are given in Tables E1 and E2[1] and are shown in Figure 2. The analyses were carried out during March 2001. The analytical procedure is described in detail elsewhere [*Shimizu and Hart*, 1982; *Shimizu*, 1998]. The polished samples were gold

Table 1. Point Counting Results

Nodule	N	Ol	Cpx	Plg	Chr
JM02n2	-	100	-	-	tr
JM01n1	-	100	-	-	tr
JM01n2	-	100	-	-	tr
FH98-42	158	34	66	-	tr
JM03n1	73	73	27	-	-
JM23n1	64	19	81	-	-
JM33n1	29	76	24	-	tr
JM06n1	69	22	29	49	-
JM21n1	110	8	20	72	-
JM32n1	94	24	49	27	-
JM25n1	46	2	39	59	-
JM20n1	151	7	59	34	-
JM14n1	92	2	4	94	tr
JM02n1	64	44	17	39	tr
JM08n1	43	44	30	26	tr
JM04n1	101	1	81	18	-
JM11n1	164	1	1	98	-
JM17n1	49	59	16	24	tr
JM12n1	71	83	-	17	-
JM18n1	107	14	-	86	-
JM29n1	80	9	-	91	-
JM09n1	183	-	4	96	-
JM39n1	81	-	48	52	-
JM03n2	39	-	44	56	-
Mean dunite	-	100	-	-	tr
Mean wehrlite	324	50	50	-	tr
Mean ol + cpx + plg	983	20	31	49	tr
Mean ol + plg	258	35	-	65	-
Mean cpx + plg	303	-	32	68	-
Mean plg-free	324	72	28	-	tr
Mean plg-present	1544	19	26	55	tr

Volume percentage of minerals in individual nodules. The number of points counted for each nodule, N, was limited by the nodule size. Mg-Al-chromite was present in several of the nodules, typically present as inclusions in olivine. The presence of such chromite is marked by a 'tr' in the column headed 'Chr'.

coated and then bombarded by a beam of negatively charged oxygen ions (O^-) with a net voltage of ~12.5 kV. Near circular beams with diameters of 20 μm were used for melt inclusion analyses and beams of up to 100 μm were used for clinopyroxene analyses. Molecular ion interferences were suppressed using the energy filtering technique [*Shimizu and Hart*, 1982], so the secondary accelerating voltage was offset by 90 V for REE analysis and 60 V for other elements. Element abundances were calculated by converting secondary ion intensity (ratioed to ^{30}Si) with empirical relationships between intensity and concentration; the specific relationship used here was calculated from an enlarged version of the database developed by *Johnson et al.* [1990] for basalt glasses. The precision and accuracy were estimated

using repeat analyses of sample melt inclusions and clinopyroxenes, a Hawaiian basalt glass internal standard (KL-2) and a Kilbourne Hole peridotite clinopyroxene standard (KH-1). The precision estimates obtained from 16 repeat analyses of sample melt inclusions and 15 repeat analyses of sample clinopyroxenes and are shown in Table 7. The precision estimates for the melt inclusions are similar to those found in two previous studies of Borgarhraun melt inclusions using the same machine, with light REEs having a precision of 10–15% and heavy REEs having one of 5–10% [*Slater et al.*, 2001; *Maclennan et al.*, 2003]. *Shimizu* [1998] found that the accuracy estimates are similar to the precision estimates.

2.2.2. EMP Analyses

[9] The concentrations of major and selected minor elements in the crystals and melt inclusions were determined using a Cameca SX50 electron microprobe at the University of Cambridge. A review of electron microprobe methods is given by *Reed* [1996]. The olivines that had been set in epoxy and the thin sections of the nodules were polished and carbon coated. The concentrations of the major elements were determined in energy dispersive (ED) mode with a count time of 60 s. Quantitative ED analysis uses the ZAF4 least squares profile fitting technique and stored elementary peak profiles from standards such as periclase (Mg), pure iron (Fe), wollastonite (Ca, Si) and corundum (Al). The probe was calibrated with these standards before the start of each session. The accuracy and precision for major elements present at >5 wt% oxide is ~1% (1σ relative precision) for ED analysis; the precision can be calculated from the counting statistics as described by *Reed* [1996]. For olivine and clinopyroxene analyses the concentrations of Ni, Na, Ca and Cr were measured using wavelength dispersive spectroscopy (WDS). During the WDS analysis a count time of 60 s was used on the peak and 20 s on the background. For melt inclusion analysis the beam width was 5 μm with a current of 3 nA and acceleration voltage of 20 kV. For olivine and clinopyroxene analyses a current of 25 nA was used and for plagioclase analyses a current of 15 nA. Samples with totals outside the range 99–101% were discarded. Esti-
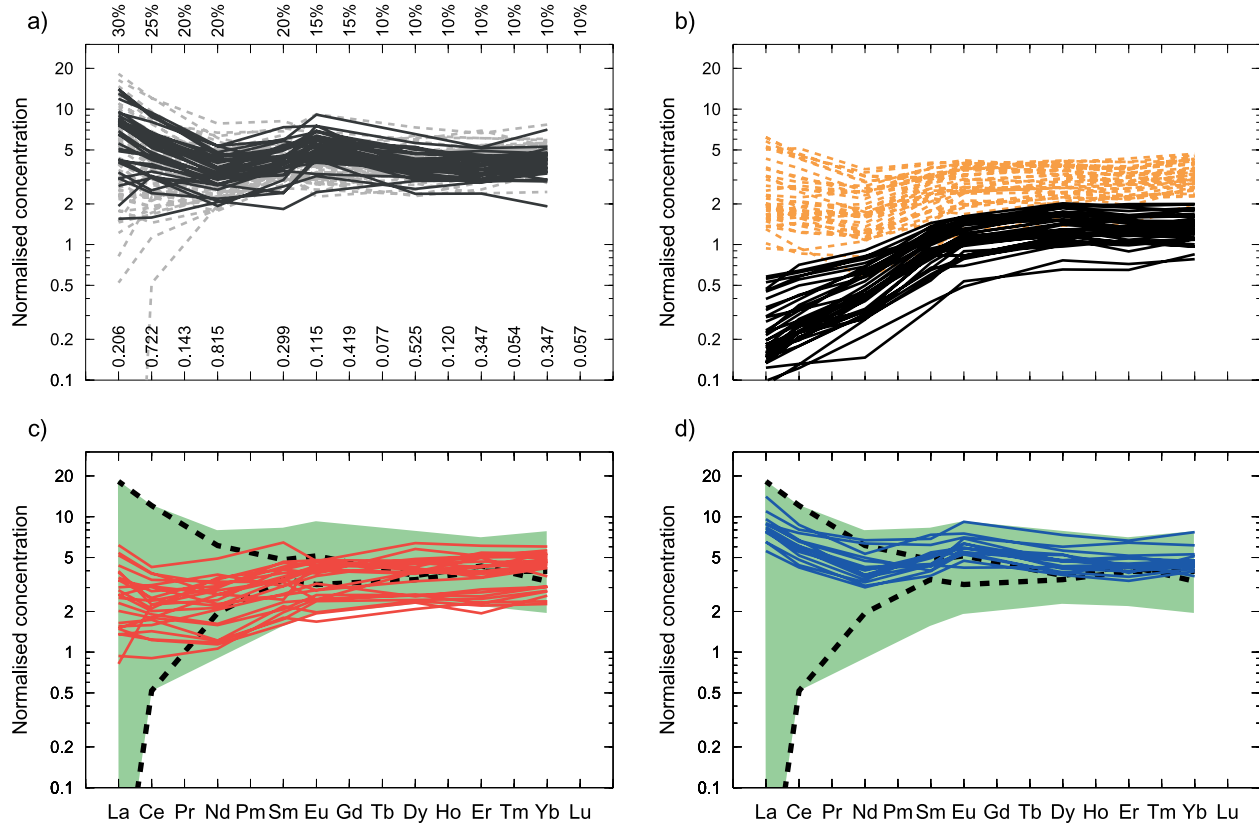
Figure 2. Depleted mantle source normalized REE measurements (a) Olivine hosted melt inclusion compositions from Borgarhraun nodules are shown as black lines. Borgarhraun phenocryst olivine-hosted melt inclusions from *Slater et al.* [2001] and *Maclennan et al.* [2003] are shown as grey dashed lines. The values at the bottom of the plot show the composition of the depleted mantle source of *McKenzie and O'Nions* [1991] that is used for normalization and those at the top show the estimated error on this source composition. (b) Borgarhraun nodule clinopyroxene compositions are shown as black lines. The orange lines show the range of melt compositions in equilibrium with the clinopyroxenes, calculated using the method of *Wood and Blundy* [1997] as described in section 4.2 of the text. (c) Green field shows that total range of composition of melt inclusions hosted in olivines with forsterite contents <90.6. The red lines show the compositions of melt inclusions hosted in olivines with >90.6. The upper black dashed line shows the composition of the melt inclusion with the highest La/Yb, and the lower one shows the composition of the melt inclusion with the lowest La/Yb. (d) Same as Figure 2c, except that the blue solid lines show the composition of melt inclusions hosted in olivines with forsterite contents of <87.5.

mates of the precision of the EMP analyses are given in Table 6 and show that for olivines the Mg# precisions are better than 0.3% relative and Ni and Ca are better than 5% relative and for clinopyroxene the Mg# precisions are better than 0.2% relative and Cr and Na are better than 4% relative.

[10] The results of the EMP analyses are shown in Tables E3, E4 and E5[1]. Elements whose peak

heights were less than three standard deviations of the background count are not given in this table. The compositions of Borgarhraun nodule crystals and phenocrysts are shown in Figures 3, 4, and 5.

2.2.3. Oxygen Isotope Analyses

[11] A number of hand-picked olivine, clinopyroxene and plagioclase crystals were selected for

Figure 3. (opposite) Compositions of mineral phases in Borgarhraun nodules. The nodule names are at the left of the plot. The green circles show measured forsterite contents in olivines, the blue unfilled squares are the Mg# of clinopyroxenes and the black crosses give X_An for plagioclase. The nodules are arranged in 5 sub-groups according to the minerals present, and within each subgroup the forsterite content of the average olivine in the nodule increases toward the bottom of the plot.
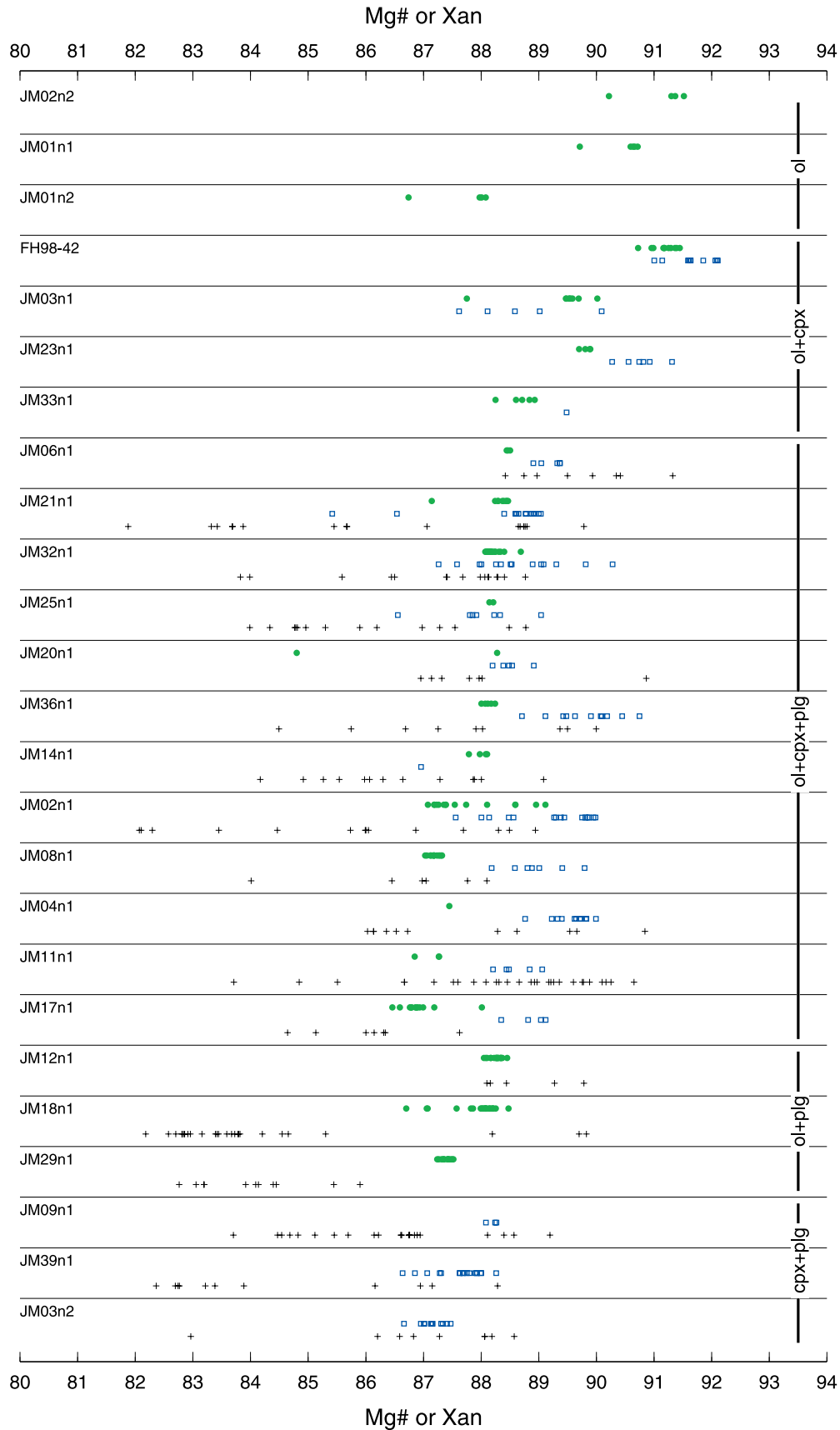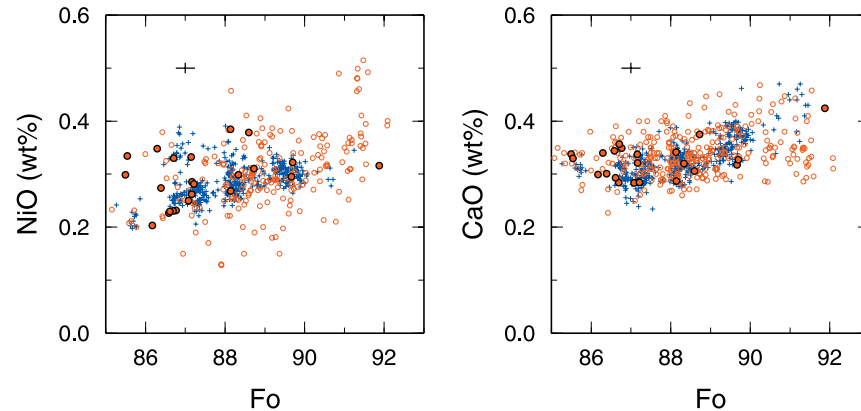
Figure 4. Comparison of olivine compositions from nodules (small blue crosses) and phenocrysts (unfilled red circles). Measurements from skeletal olivine phenocrysts are shown as filled red circles with a thick black outline. The $\pm 1\sigma$ analytical precision is shown as a black cross.

oxygen isotope analysis by laser fluorination at the California Institute of Technology. Most of the crystals analyzed had already been characterized by EMP and SIMS analyses. Crystals that had been mounted in epoxy for SIMS analysis were excavated from the epoxy and soaked in dichloromethane overnight. Then the epoxy was removed from the crystal surfaces and the crystals were cleaned in an ultrasonic bath. The crystals were then hand-picked under a binocular microscope and were seen to be free of epoxy and alteration. Several of the picked olivines contained inclusions of chromite or melt. Inspection of the polished sections with exposed inclusions showed that inclusions make up less than 3 vol% of the grain. High temperature fractionation between chromite and olivine is about 1.5 per mil. [*Chiba et al.*, 1989], so the shift caused by the inclusions is likely to be less than 0.05 per mil.. The analytical approach was similar to that used by *Eiler et al.* [2000], and the fluorination was carried out using a 50 W CO_2 laser and a BrF_5 reagent. The presence of chromite inclusions may be in part responsible for the mean oxygen yield of 90%, since olivines of the composition found in the nodules produce $\sim$13.4 μmol mg^{-1} of O_2 and chromites produce $\sim$8.6 μmol mg^{-1}. Over the five days of analysis 30 repeat measurements of standard garnet GMG2 gave $\delta^{18}O$ = 5.90 $\pm$ 0.05 per mil. and 19 repeat analysis of San Carlos Olivine SCO3 gave 5.45 $\pm$ 0.05 per mil.. All of the data were then corrected

to the accepted value of $\delta^{18}O$ = 5.75 per mil. for GMG2. The data were not corrected on a daily basis because shifts in the values of SCO3 and GMG2 did not correlate for each day. Repeat analyses of splits of 17 samples gave a reproducibility of 0.17 per mil.. It is likely that this value reflects small scale inhomogeneity in the samples. The $\delta^{18}O$ results are given in Table E6[3] and discussed in section 5.

3. Crystal, Melt and Host Rock Compositions

3.1. Relationship Between Nodule Crystals and Phenocrysts

[12] The average composition and compositional range of crystals found within the nodules and as phenocrysts is similar, as shown in Figures 4 and 5. For olivines, the field of nodule crystal compositions lies within that of the phenocrysts. It is likely that olivine phenocrysts with skeletal form grew in the Borgarhraun melt as opposed to having been incorporated from magma chamber walls. These skeletal phenocrysts again display a similar range in composition to that found in the nodule crystals. The field of clinopyroxene compositions found in the phenocrysts lies within that of the nodule clinopyroxenes. The anorthite contents of the plagioclase from both the nodules and phenocrysts is variable, and shows strong variation within single nodules and crystals. For instance, in nodule
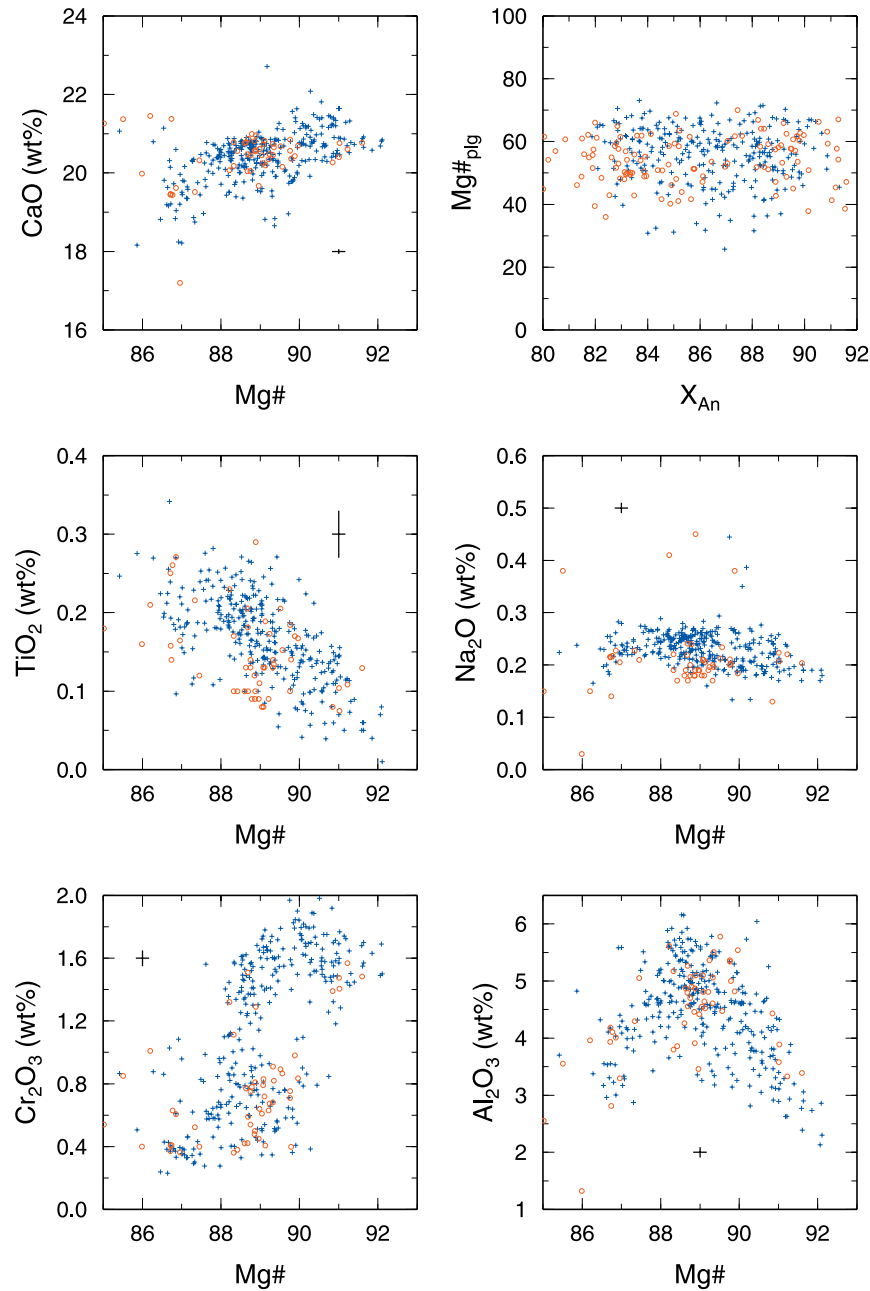
Figure 5. Comparison of mineral phases from nodules and phenocrysts, using same symbols as Figure 4. The plots are all for clinopyroxene compositions save the upper right which shows plagioclase compositions.

JM21n1 the anorthite content varies from 82 to 90 mol%, and the interior of a single plagioclase crystal from nodule JM09 shows variation in from 83 to 90 mol% anorthite within a distance of 0.4 mm. This small-scale variation may result from the growth of plagioclase from melts with variable Na contents and is preserved due to the sluggish rates of NaSi-CaAl diffusion in plagioclase [*Grove*

et al., 1984]. The similarity in the compositional range of crystals found in the nodules and phenocrysts is mirrored in the REE compositions of olivine-hosted melt inclusions. Both the range of melt inclusion compositions and the evolution of this range with decreasing Fo content of the host olivine are similar in the nodules and the phenocrysts (section 4.3).

[13] Although in some instances nodules are disaggregating to generate phenocrysts, disaggregation of the observed nodules alone cannot produce the phenocryst population in Borgarhraun, because the average modal proportion of olivine in the phenocrysts is higher than that observed in the nodules. This observation, along with that of the range in composition of skeletal olivines, indicates that it is likely that phenocrysts in Borgarhraun are generated both by disaggregation of nodules and by the growth of crystals from the melt. Furthermore, the accord between the nodule compositions and the skeletal olivine compositions suggests that the nodule olivines crystallized from melt displaying a similar range of compositions to those present in the Borgarhraun samples.

3.2. Intranodule Disequilibrium

[14] It is possible to check for equilibrium between crystals in individual nodules by comparing the measured compositional variability within single nodules with the estimated precision of the measurements. The compositional variation within individual nodules is shown in Figure 3 and is summarized in Table 2.

[15] These results show that while almost half of the nodules appear to be close to equilibrium for elements or element couples with diffusion coefficients of $\sim 10^{-16}$ m^2 s^{-1} at 1200°C, such as Ca in olivine, less than 10% of the nodules are in equilibrium for elements with diffusion coefficients of $\sim 10^{-17}$ m^2 s^{-1} or less. Disequilibrium is also observed in the oxygen isotope measurements from the nodules, both within individual phases and between phases. The equilibrium δ^{18}O fractionation between the phases at 1260°C was calculated using the method of *Chiba et al.* [1989], and gave fractionations of 0.4 per. mil. for forsterite-diopside and 0.7 per. mil. for fosterite-anorthite. The observed and calculated equilibrium olivine oxygen isotope compositions are shown in Table 3. Out of the 11 nodules where the composition of more than one phase is known, only one (JM18) approaches equilibrium. The widespread oxygen isotope disequilibrium is to be expected since the diffusion coefficients of oxygen in olivine, clinopyroxene and plagioclase at 1200°C are 10^{-19}–10^{-20} m^2 s^{-1},

much less than those for Mg-Fe interdiffusion. There is no petrographic evidence for direct interaction of the nodules with hydrothermal water, so it is possible that the disequilibrium results from magmatic processes. The presence of such disequilibrium may be accounted for if each nodule grew from melts with variable compositions, as expected from the variation of REE contents within the crystals and melt inclusions from individual nodules. The characteristic time for chemical equilibration in the nodules, t_c is given by $t_c = a^2/D$ where a is the radius of the nodule and D is the diffusion coefficient. Since the average radius of the nodules is ~ 1 cm, then the presence of disequilibrium in elements with a D of 10^{-17} m^2 s^{-1} or less indicates that the nodules cannot have been held at 1200°C for over 10^5 years.

3.3. Relationship Between Melt Inclusions, Olivines and the Host Flow

[16] Theistareykir whole rock sample compositions show a wide range in both major element and incompatible trace element concentrations. These whole-rock compositions can be compared with olivine compositions after the whole-rock composition has been converted into an equilibrium olivine composition (see Figure 6 for details). Over 80% of the olivine analyses from Borgarhraun phenocrysts or nodules are in equilibrium with melts that have the compositions of the Borgarhraun whole-rock samples [*Slater et al.*, 2001; *Maclennan et al.*, 2002]. However, many of the whole-rock samples contain accumulated olivines and olivines within individual samples have variable compositions, so it is unlikely that the majority of individual olivines were in equilibrium with the melt in their host sample.

[17] Despite this lack of equilibrium between Borgarhraun olivines and their host melts, inspection of Figure 6a shows that these olivines crystallised from melt whose average composition was closer to that of Borgarhraun than to that of any other flow from Theistareykir or Krafla. Of the 22 Theistareykir flows analyzed by *Slater* [1996], only 3 have both whole rock sample REE compositions close to that of the Borgarhraun mean melt inclusion composition and major element compo-

Table 2. Summary of Variability Within Selected Nodules

Nodule	Ol				Cpx			Plg	
	Mg#	CaO	NiO	La$_{mi}$	Mg#	CaO	Yb	An#	CaO
JM03	89.40 ± 0.64	0.33 ± 0.02	0.30 ± 0.02	-	88.68 ± 0.94	20.10 ± 0.44	-	-	-
JM04	-	-	-	-	89.55 ± 0.35	20.10 ± 0.48	0.49 ± 0.09	87.71 ± 1.74	17.75 ± 0.39
JM05	**89.03 ± 0.12**	**0.32 ± 0.00**	**0.29 ± 0.01**	-	88.79 ± 0.37	20.53 ± 0.16	**0.50 ± 0.02**	-	-
JM07n1	**89.92 ± 0.06**	**0.37 ± 0.01**	**0.30 ± 0.01**	1.54 ± 0.72	90.69 ± 0.43	20.67 ± 0.13	0.39 ± 0.05	-	-
JM07n2	-	-	-	-	90.87 ± 0.37	20.55 ± 0.13	0.40 ± 0.05	-	-
JM08	-	-	-	-	88.95 ± 0.53	19.90 ± 0.22	-	86.73 ± 1.46	17.57 ± 0.31
JM09	-	-	-	-	**88.20 ± 0.10**	20.36 ± 0.08	-	86.33 ± 1.44	17.42 ± 0.30
JM11	-	-	-	-	88.61 ± 0.34	20.05 ± 0.32	-	89.07 ± 2.42	17.93 ± 0.57
JM13	-	-	-	-	88.41 ± 1.03	20.14 ± 0.20	0.53±0.12	-	-
JM15	**87.89 ± 0.14**	**0.29 ± 0.00**	**0.28 ± 0.01**	-	-	-	-	-	-
JM16	**88.37 ± 0.12**	**0.32 ± 0.00**	**0.27 ± 0.01**	-	-	-	-	-	-
JM17n1	86.92 ± 0.36	0.29 ± 0.04	0.34 ± 0.03	**1.63 ± 0.17**	88.88 ± 0.69	20.07 ± 0.30	0.61 ± 0.10	-	-
JM17n2	**89.29 ± 0.12**	**0.35 ± 0.01**	**0.30 ± 0.01**	2.23 ± 0.68	-	-	-	-	-
JM18	87.93 ± 0.43	0.31 ± 0.02	0.31 ± 0.02	-	-	-	-	84.11 ± 2.03	17.03 ± 0.43
JM29	**87.39 ± 0.09**	**0.32 ± 0.01**	0.25 ± 0.02	-	-	-	-	84.05 ± 0.99	17.76 ± 0.17
JM41	**89.68 ± 0.08**	**0.33 ± 0.01**	**0.31 ± 0.01**	**0.61 ± 0.16**	89.93 ± 0.82	20.31 ± 0.16	0.41 ± 0.10	-	-
1σ error	0.24	0.01	0.01	0.23	0.17	0.06	0.04	-	0.10
D (m^2 s^{-1})	10^{-16}	10^{-16}	10^{-16}		10^{-18}	10^{-17}	10^{-19}	10^{-21}	-

The compositional variability within single phases from selected nodules is shown as mean with 1σ errors. The column headed La$_{mi}$ is the variability of melt inclusion compositions hosted within the nodule. The row labelled 1σ error shows the measurement precision as given in Tables 6 and 7. The row marked D shows the diffusion coefficient for the element in the phase at a temperature of 1200°C [*Chakraborty*, 1997; *Jurewicz and Watson*, 1988; *Ito et al.*, 1999; *Dimanov and Sautter*, 2000; *Dimanov et al.*, 1996; *Van Orman et al.*, 2001; *Grove et al.*, 1984]. The fields marked bold show where the observed variation is less than the precision, and the nodule may be in equilibrium for the quantity.

Table 3.   Summary of Nodule Oxygen Isotope Results

Nodule	Ol		Cpx			Plg		
	Obs	Av	Obs	Av	Ol_{eq}	Obs	Av	Ol_{eq}
JM03	*4.68*	**4.68**	*4.49*	4.49	**4.09**	-	-	-
JM04	-	-	*4.84, 4.84*	4.84	**4.44 ± 0.00**	-	-	-
JM05	4.43, 4.42	**4.42 ± 0.01**	*4.46*	4.46	**4.06**	-	-	-
JM07n1	5.17, 5.04, 5.10 5.06 *4.91, 5.09, 5.13*	**5.07 ± 0.08**	5.20	5.20	**4.79**	-	-	-
JM07n2	-	-	*4.88, 4.88*	4.88	**4.48 ± 0.00**	-	-	-
JM08	-	-	-	-	-	*4.98, 5.02*	5.00	**4.26 ± 0.03**
JM09	-	-	*4.47*	4.47	**4.07**	3.87, 3.83, 3.93	3.88	**3.15 ± 0.05**
JM11	-	-	*4.57, 4.70*	4.63	**4.23 ± 0.09**	*5.20*	5.20	**4.46**
JM13	-	-	-	-	-	5.25	5.25	**4.51**
JM15	4.88, 4.82	**4.85 ± 0.04**	4.95, 4.70	4.82	**4.42 ± 0.18**	-	-	-
JM16	*5.13*	**5.13**	*4.74*	4.74	**4.34**	-	-	-
JM17n1	4.87, 4.93	**4.90 ± 0.04**	-	-	-	-	-	-
JM17n2	3.50, 3.44, 3.71 3.41	**3.51 ± 0.14**	-	-	-	-	-	-
JM18	*4.32, 4.22*	**4.27 ± 0.07**	-	-	-	*5.12*	5.12	**4.37**
JM29	*4.05*	**4.05**	-	-	-	5.35, 5.42, *5.01*	5.26	**4.52 ± 0.22**
JM41	*4.32, 4.23*	**4.27 ± 0.06**	*4.77, 5.07*	4.92	**4.52 ± 0.21**	-	-	-

The columns marked Obs show the individual δ^{18}O observations. Values not in italic are from individual crystals, while values in italic are from composite samples of many crystals from the nodule. The averages are given in the columns Av. The composition of olivines in equilibrium with the clinopyroxene or plagioclase averages were calculated using the fractionation coefficients of *Chiba et al.* [1989] for a temperature of 1260°C.

sitions that are in equilibrium with olivines with a similar average composition to those that host the melt inclusions (Figure 6). These three flows are Langaviti, Hoefudreidarmuli and Borgarhraun itself. This compositional similarity indicates that most of the Borgarhraun phenocrysts and nodules crystallized either from the Borgarhraun melt, or from a melt with a composition close to that of Borgarhraun. This similarity persists after correction of the whole-rock compositions for olivine accumulation of ~10%, which lower Fo contents of the calculated equilibrium olivine composition by ~2 mol%. The overlap in the range of skeletal olivine and nodule or non-skeletal phenocryst olivine compositions also indicates that the nodule and phenocryst olivines grew from melts with similar compositions to Borgarhraun (Figure 4).

[18] The average composition of melt inclusions found in olivines with Fo > 90.6 is similar to those of picrites erupted 10 km to the northwest of Borgarhraun. These melt inclusions may have been trapped in wehrlites that were formed by crystallization of magma bodies with the same average composition as the picrites. Alternatively, picritic melts may have been present in the Borgarhraun

magma body before mixing, so that crystallization of these melts produced forsteritic olivines with inclusions of low La melt. The Borgarhraun nodules and phenocrysts are not random samples of the Theistareykir crust and may have been produced by crystallization within the magma body or bodies that erupted to create Borgarhraun.

3.4. Conditions of Crystallization

[19] Although Mg-Fe and Ca disequilibrium is present within individual nodules (section 3.2), both the average Mg# and the average CaO content of olivines and clinopyroxenes from individual nodules are correlated (Figure 7). This overall correlation between olivine and clinopyroxene compositions may be produced by fractional crystallization of a single well-homogenized melt batch that initially crystallizes olivine and clinopyroxene with a Mg# of ~92 and evolves toward lower Mg# along a liquid line of descent (LLD). However, the Mg# correlation is dominated by the two extreme points, and there is scatter at Fo$_{88-90}$. The presence of this scatter, and the lack of equilibrium within individual nodules, shows that the LLD model does not account for the all of the compositional
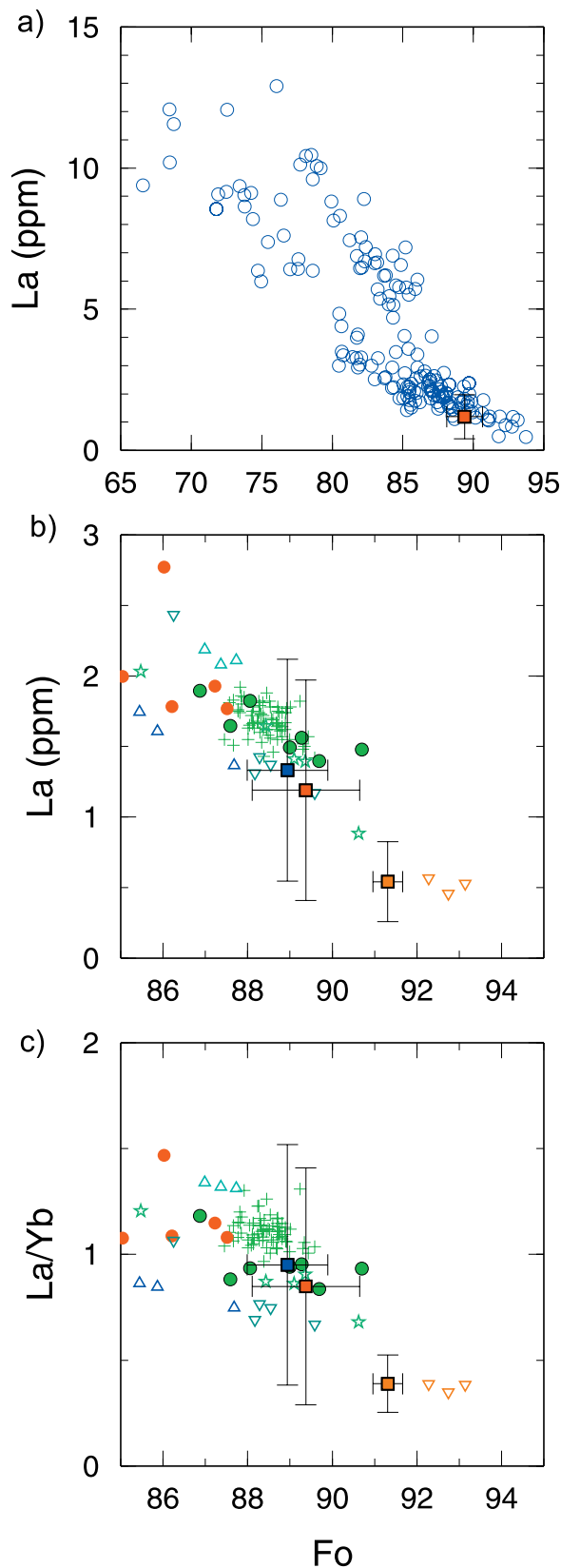
variation within the Borgarhraun nodules. Such scatter may be generated by the growth of individual nodules from melts of variable composition, consistent with the variation in melt inclusion compositions (section 4) and the variation in oxygen isotope ratios (section 5) within single nodules. Another cause of the scatter may be partial re-equilibration of Mg-Fe and Ca between olivine and clinopyroxene over a range of temperatures.

[20] Inspection of Figures 3 and 7 and Table 1 shows that there is a relationship between the mineral compositions and the modal mineralogy of the nodules. The maximum olivine forsterite content found in both dunitic and wehrlitic nodules is ~91.6 and the maximum mean forsterite content in any wehrlitic nodule is 91.2. However, the maximum forsterite content observed in any plagioclase-bearing nodule is 89.1, and the maximum

Figure 6. (opposite) (a) Plot of all Theistareykir glacial and postglacial compositions reported by *Maclennan et al.* [2002] from *Slater* [1996] are shown as blue circles. The La concentration is that of the whole rock sample and the Fo content is that calculated to be in equilibrium with the whole rock composition at a temperature of 1200°C and a pressure of 0.8 GPa using the method of *Ford et al.* [1983]. The calculated K_d^{Fe-Mg} was 0.32 ± 0.01. The Fe^{3+} to Fe^{2+} ratio of the melt was calculated at an oxygen fugacity one log unit beneath the quartz-fayalite-magnetite buffer using the method of *Kilinc et al.* [1983]. This method gave an average Fe^{2+}/Fe^{tot} of 0.90 ± 0.01. The red filled square shows the mean composition of the Borgarhraun melt inclusions and their host olivines with the error bars showing 1σ. (b) Detailed comparison between average Borgarhraun melt inclusion compositions and Theistareykir whole-rock compositions. The whole rock data in this plot are the high precision measurements of *Stracke et al.* [2003] of primitive Theistareykir samples and the Borgarhraun analyses of *Maclennan et al.* [2003]. The red filled square is the mean melt inclusion and host olivine composition, the blue filled square is the mean in host olivines with Fo < 90.6, and the brown filled square is the mean in host olivines with Fo > 90.6. The whole rock symbols are as follows. Brown downward pointing triangles, picrites; dark green downward pointing triangles, Hoefudreidarmuli; blue upward pointing triangles, Arnahvammurhraun; turquoise upward pointing triangles, Bondholshraun; small red filled circles, Storaviti; green stars, Langaviti; filled green circles, Borgarhraun [*Stracke et al.*, 2003]; green crosses, Borgarhraun [*Maclennan et al.*, 2003]. (c) Same key as for Figure 6b.
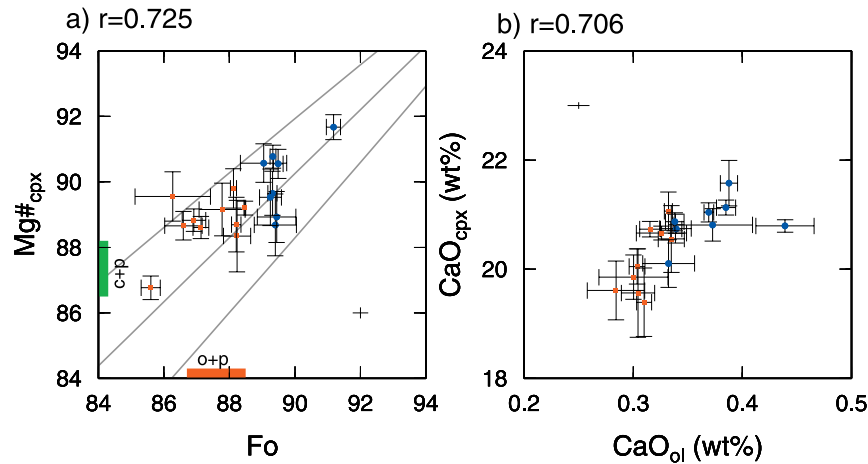
Figure 7. Average clinopyroxene compositions plotted against average olivine compositions from nodules where clinopyroxene and olivine are both present. The error bars show 1σ variation within individual nodules. Red squares show nodules where plagioclase is present, blue circles show those where only clinopyroxene and olivine are present. The cross without a point shows the 1σ analytical precision. The red bar marked o + p in Figure 7a shows the range of olivine compositions found in the troctolites, while the green bar marked c + p shows the range of clinopyroxene compositions in olivine-free gabbros. The grey lines in Figure 7a show the equilibrium Fe-Mg partitioning calculated using the method of *Loucks* [1996], for temperatures of 1160°C (upper line), 1210°C and 1260°C.

average forsterite content in such nodules is 88.5. The presence of high Fo olivines in wehrlites and lower Fo olivines in gabbros indicates that clinopyroxene joins the crystallizing assemblage before plagioclase. This order of crystallization is consistent with the relationship between clinopyroxene Mg# and modal mineralogy. While the average Mg# of clinopyroxenes in wehrlites reaches 91.7, the maximum average Mg# of clinopyroxenes in gabbros is 89.8. There is an overlap in the Mg# of clinopyroxenes found in wehrlites and gabbros and this overlap is likely to be caused by compositional variability within the melts that crystallized individual nodules and leading to disequilibrium between the phases in these nodules. However, this variability is not sufficiently large to obscure the overall relationship between modal mineralogy and mineral compositions.

[21] Crystallisation experiments have shown that MORB-like compositions start to precipitate clinopyroxene before plagioclase at pressures of >0.8 GPa [*Bender et al.*, 1978]. This pressure estimate is confirmed by crystallization modelling using the method of *Weaver and Langmuir* [1990]. Melts with the composition of the average Borgarhraun whole-rock sample crystallise olivine and clinopyroxene between Fo$_{91}$ and Fo$_{88}$ and

olivine, clinopyroxene and plagioclase at lower forsterite contents only when pressures are >0.8 GPa. The water contents of Borgarhraun melts are approximately 0.15 wt% (E. Hauri, personal communication, 2002) and such small water contents have little effect on the order of crystallization [*Danyushevsky*, 2001].

[22] The relationship between the modal mineralogy and olivine compositions within the nodules can be produced if the Borgarhraun nodules were generated by fractional crystallization at pressures of >0.8 GPa. The compositions of Borgarhraun clinopyroxene phenocrysts and whole-rock samples and the compositional trends present in Theistareykir basalts are also consistent with fractional crystallization of Borgarhraun melt at pressures of close to 0.9 GPa [*Maclennan et al.*, 2001a; *Maclennan et al.*, 2003]. Wehrlite bodies are found in the Moho Transition Zone (MTZ) of the Oman ophiolite, indicating that wehrlites can be generated at pressures of under 0.3 GPa [*Koga et al.*, 2001]. However, the Oman MTZ cumulates have different compositional relationships to those of the Borgarhraun nodules, with large overlaps in the olivine compositions found in gabbros (Fo$_{78-88}$) and wehrlites (Fo$_{80-89}$). No such overlap exists in the Borgarhraun samples. Furthermore, the most for-

steritic olivines in the Oman MTZ are found in troctolites (Fo$_{89-90}$) and dunites (Fo$_{88-91}$), while the Borgarhraun troctolites have less forsteritic olivines (Fo$_{87-88}$) than the Borgarhraun wehrlites (Fo$_{89-91}$). These relationships indicate that Oman MTZ gabbros and wehrlites crystallized from melts of similar Mg#, and that Oman melts were saturated in plagioclase at smaller extents of crystallization than clinopyroxene, as expected for low pressure crystallization of melts with compositions similar to MORB.

[23] Temperatures of olivine-clinopyroxene equilibration in the nodules can be estimated by applying the Mg-Fe exchange thermometer of *Loucks* [1996] and the Ca exchange thermobarometer of *Kohler and Brey* [1990] to the average olivine and clinopyroxene compositions from individual nodules. For the Mg-Fe exchange calculations all of the iron present in clinopyroxene was assumed to be present as Fe^{2+} and equilibrium temperature estimates range from 1150 to 1240°C. If only 90% of the iron is present as Fe^{2+} then the temperature range drops to 1140 to 1220°C. A pressure of 0.8 GPa was assumed for the Ca exchange thermometer and equilibrium temperature estimates were 1260–1280°C. These temperatures are similar to those of ~1260°C estimated for crystallization of the Borgarhraun clinopyroxene phenocrysts using the clinopyroxene-melt thermometer of *Putirka et al.* [1996], which has a 1σ calibration error of ±40°C. Both of these thermometers are based on equilibration between olivine and clinopyroxene, and the presence of Mg-Fe and Ca disequilibrium within nodules leads to uncertainty and the temperature estimates should be interpreted with caution (Table 2). While a number of time-temperature histories could generate such high equilibration temperatures, the model equilibration at magmatic temperatures is expected if the nodules formed by crystallization of the Borgarhraun melt, as suggested in section 3.3.

3.5. Causes of Variation in Crystal Composition

[24] The compositional variations present in olivine and clinopyroxene crystals from Borgarhraun may result from fractional crystallization and incomplete mixing of mantle melts. Olivine compositions show a poorly defined drop in NiO with decreasing Fo content, which may be generated by fractional crystallization (Figure 4). Similarly, the increase in TiO$_2$ and drops in Cr$_2$O$_3$ and Al$_2$O$_3$ with decreasing Mg# in clinopyroxenes with Mg# < 89 may result from fractional crystallization of gabbroic material (Figure 5). However, the scatter in NiO in olivines and TiO$_2$, Cr$_2$O$_3$ and Al$_2$O$_3$ in clinopyroxenes at fixed Mg# cannot be produced by isobaric fractional crystallization of melts with the same starting composition. This scatter may reflect either variation in the composition of the parental melts or variation in the crystallization conditions which alters partitioning of elements between melt and crystals [e.g., *Ford et al.*, 1983; *Putirka*, 1999].

[25] At Mg#s between 92 and 89 clinopyroxenes show a broad increase in Al$_2$O$_3$ with decreasing Mg#, so that at Mg#~92 the Al$_2$O$_3$ of the clinopyroxenes are 2–3 wt% and at Mg#~89 the range is 3–6 wt%. Melting experiments on mantle peridotite composition MM3 show that at melt fractions of <5% the Mg# of the melts generated are low (<74.3) and the Al$_2$O$_3$ contents are high (>18 wt%) while at melt fractions of over 25% the Mg#s are high (up to 79.1) and the Al$_2$O$_3$ contents are as low as 12 wt% [*Baker and Stolper*, 1994; *Baker et al.*, 1995; *Hirschmann et al.*, 1998]. Therefore the crystallization of clinopyroxene from an array of unmixed melts produced at 0–25% melting would generate high Mg# clinopyroxenes (Mg#~90) with Al$_2$O$_3$ of the clinopyroxenes increasing as their Mg# decreases by ~2 Mg# units. This relationship is similar to that observed in the high Mg# clinopyroxenes from Borgarhraun, and it is possible that these clinopyroxenes crystallized from melts produced by variable degrees of mantle melting prior to extensive mixing of the primary melts. The increase in TiO$_2$, decrease in Cr$_2$O$_3$ and limited variation in CaO contents of high Mg# clinopyroxenes with decreasing Mg# are also qualitatively similar to the trends observed in the MM3 melting experiments. However, these experiments show large variation in Na$_2$O contents while the Borgarhraun clinopyroxenes have almost constant Na$_2$O contents. The MM3 melting experiments were carried out at 1 GPa, where Na is strongly incompatible, allowing large
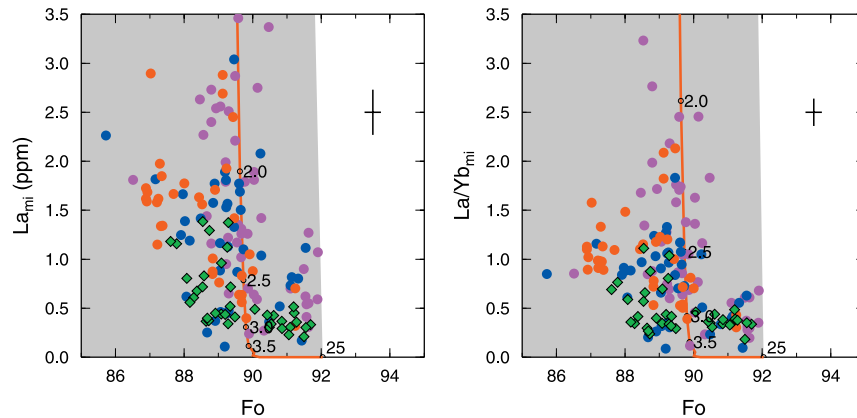
Figure 8. REE compositions of Borgarhraun melt inclusions plotted against forsterite content of their host olivines. The blue circles show the phenocryst data of *Maclennan et al.* [2003], the purple circles the phenocryst data of *Slater et al.* [2001] and the red circles the nodule data from this work. The green diamonds show the nodule clinopyroxene compositions converted into melt and equilibrium olivine composition as described in the text. The red line shows the path of instantaneous fractional melt compositions from the melting model in Figure 11. The line is labeled with the percent of melting required to generate the melt compositions. The first melts are in equilibrium with a Fo_{89} olivine and have a La content of 43 ppm and a La/Yb ratio of 61 and are too extreme to be displayed on these plots. The grey region shows the field of all possible melt/olivine compositional pairs that can be generated by mixing and fractional crystallization of the predicted instantaneous fractional melt compositions. The black cross shows the 1σ analytical precision calculated from repeat measurements.

Na variation to be generated. At higher pressures, similar to those of $3-4$ GPa expected for the onset of melting under Theistareykir [e.g., *Slater et al.*, 2001], Na is much less incompatible during mantle melting, and mantle melts will show less variable Na contents (see compilation in *Longhi* [2002]). Major element variability in mantle melt composition may also be generated by compositional variation within the mantle source [e.g., *Robinson et al.*, 1998; *Hirschmann et al.*, 1999].

[26] While the variation in major element composition of the Borgarhraun crystals may record the composition of unmixed mantle melts, comparison of the results of melting experiments and the crystal composition suffers two key problems. Firstly, the melting experiments involve isobaric batch melting, while melting in the mantle is thought to be similar to polybaric fractional melting. Secondly, the crystal compositions only provide an indirect record of the melt compositions because the crystal composition is controlled both by the partitioning behavior of the element and by its concentration in the melt. Variation in the partitioning can be caused by changes in the conditions of crystallization. Fortunately, these problems are not as important for REE composi-

tions of olivine-hosted melt inclusions and in the next section melt inclusion compositions are used to infer that mantle melts were not fully mixed before crystallization of the olivine and clinopyroxene crystals.

4. Melt Mixing and Crystallization

4.1. Variation of Melt Inclusion and Host Olivine Compositions

[27] Both the average composition and compositional range of REEs in the melt inclusions vary according to the forsterite content of the host olivine, as shown in Figures 2 and 8. It is likely that the reduction of compositional variation with decreasing forsterite content of the host olivine reflects concurrent mixing and crystallization, and it is clear that mixing is not complete before the onset of crystallization. The data cannot be accounted for by a liquid line of descent from a single primary melt composition. One or more mixing events can be observed in the Borgarhraun melt inclusion data. An impressive evolution in REE variability with decreasing forsterite content is recorded in olivines with forsterite contents between $Fo_{90.6}$ and Fo_{86}. The range in La/Yb ratio

of the melt inclusions in olivines of Fo$_{\sim90}$ is 0.1–2.4, while the La/Yb ratio in melt inclusions hosted in olivines with Fo$_{\sim86}$ is ~1 (Figure 8b). Another mixing event may be recorded in olivines with forsterite contents between Fo$_{92}$ and Fo$_{90.6}$, where the melt inclusions within the most forsteritic olivines have La contents of 0.2–1.3 ppm, but the least forsteritic olivines contain melt inclusions with La contents between 0.3–0.45 ppm (Figure 8a).

[28] Further variation in melt inclusion compositions is shown for REE concentrations, ratios and principal components in Figures 9 and 10. The use and calculation of principal components in the study of melt inclusion REE concentrations in Theistareykir basalts has been thoroughly described by both *Slater et al.* [2001] and *Maclennan et al.* [2003]. One advantage of plotting the principal components is that they reflect the overall variation in the 8 measured REEs, and the first two principal components describe approximately 80% of the total variance of the REE data set. Therefore plots of the principal components confirm that the changes in compositional variability as a function of host olivine composition are an overall feature of the REE data rather than being restricted to a limited number of elements. The approach used here differs slightly from that of *Maclennan et al.* [2003] in that principal components for REE/Yb ratios were calculated in addition to those for the raw concentrations, because REE/Yb ratios are not strongly influenced by fractional crystallization. The principal components for the REE concentrations are shown in Table 4 and those for the REE/Yb ratios are in Table 5. The first principal component for the REE concentrations is sensitive to uniform increases in concentration, while the second principal component is high for melt inclusions with high light REE contents and low heavy REE contents (Table 4).

4.2. Variation in Clinopyroxene Compositions

[29] Clinopyroxene REE compositions can be compared with those of the melt inclusions by determining the equilibrium melt composition for each clinopyroxene. The method of *Wood and Blundy* [1997] was used to calculate the partition coeffi-

cients, Ds, of the REEs in the Borgarhraun clinopyroxenes and this method requires estimates of pressure, temperature and the major element composition of the clinopyroxene. The clinopyroxene major element compositions are known from the EMP analyses and pressure and temperature estimates of 1 GPa and 1300°C respectively were used in order to give partition coefficients for crystallization close to the base of the Theistareykir crust [*Maclennan et al.*, 2001a; *Maclennan et al.*, 2003]. The calculated partition coefficients vary from 0.08–0.09 for La, from 0.33–0.38 for Sm and from 0.40–0.44 for Yb. The clinopyroxene Mg# was converted into a melt Mg# using step 9 from the appendix of *Wood and Blundy* [1997], and the equilibrium olivine composition was then calculated using the method of *Ford et al.* [1983]. The REE composition of the melt and the forsterite content of the olivine in equilibrium with the clinopyroxenes are shown as green diamonds in Figure 8. The converted clinopyroxene compositions lie within the range of observed melt inclusion/host olivine compositional pairs from both Borgarhraun phenocrysts and nodule crystals. These calculated compositions show low values and limited variation of La and La/Yb at Fo > 90 mol%, while at lower equivalent Fo contents there is greater variability in La and La/Yb. This behavior mirrors that observed in the melt inclusions, and indicates that the clinopyroxenes grew from melts similar to those which are now included in the olivines and that the clinopyroxene and melt inclusion compositions record the same mixing histories. While the melts that are predicted to be in equilibrium with the clinopyroxenes have REE concentrations that lie within the range observed for melt inclusions, they have a lower average La concentration and La/Yb ratio and smaller compositional range than the melt inclusions. These differences may be caused by systematic errors in the estimation of partition coefficients, or may indicate that clinopyroxene preferentially grew from melts with relatively low La/Yb ratios.

4.3. Generation of the Variation in REE Contents

[30] Both *Slater et al.* [2001] and *Maclennan et al.* [2003] demonstrated that the range in REE compositions of Borgarhraun olivine-hosted melt inclu-

sions can be generated by incomplete mixing of instantaneous fractional melts from a Theistareykir melting model (Figure 11). This melting model can match both the volume-average REE composition of the Theistareykir magmas and the crustal thickness of 21 km observed by seismic surveys of Theistareykir [*Staples et al.*, 1997]. Melting starts at depths of greater than 150 km in the model and the extent of mantle melting rises from ~4 wt% at 100 km depth to ~27 wt% at 20 km. A homogeneous mantle source composition was used which is slightly more enriched than the depleted mantle source of *McKenzie and O'Nions* [1991], having a La concentration of 0.258 ppm and a Yb concentration of 0.351 ppm [*Maclennan et al.*, 2001b]. The range of REE concentrations in the predicted instantaneous melt compositions is shown in Figure 11b and these compositions were calculated as described in *Slater et al.* [2001]. The MgO and FeO contents of the instantaneous fractional melt compositions from the melting model were estimated using the parameterization of *Watson and McKenzie* [1991]. These melt compositions were then converted into equilibrium olivine compositions by assuming that 90% of Fe is present as Fe^{2+} and a K_d^{Fe-Mg} of 0.3, similar to the values estimated using the methods of *Ford et al.* [1983] and *Kilinc et al.* [1983] given in Figure 6. These equilibrium olivine compositions are shown on Figure 11b. The red line on Figure 8 shows the track of the model instantaneous melt compositions and their equilibrium olivines. The grey shaded area to the right of the line shows the field of compositions that can be generated by mixing of the instantaneous fractional melts. Melt inclusion compositions trapped in olivines that lie to the left of the red line cannot be produced by mixing of these model instanta-

neous fractional melt compositions alone and can only be matched if fractional crystallization of mafic phases, which will reduce the Mg# of the melt and hence the Fo of the equilibrium olivine, has taken place along with the mixing. All of the observed points lie within the grey area, so it is possible to account for the range of melt inclusion compositions and those of their host olivines by mixing of instantaneous fractional melts and fractional crystallization.

[31] The melts generated at greatest depth at the onset of melting have high La contents and La/Yb ratios and are in equilibrium with $Fo_{\sim89}$ olivines (Figure 11b). As melting progresses at shallower levels the modelled La contents of the instantaneous melts drop, and once 4% melting has taken place La has been exhausted from the mantle source and the instantaneous fractional melts contain no La. At this point the instantaneous melts are in equilibrium with Fo_{90} olivines. This large range of predicted instantaneous fractional melt compositions that are in equilibrium with Fo_{89-90} olivines can account for the large range in La contents observed in Borgarhraun melt inclusions hosted by $Fo_{88.5-90}$ olivines. Instantaneous melts that are produced at extents of melting greater than 4% are predicted to contain no La and to be in equilibrium with Fo_{90-92} olivines. While the observed melt inclusions trapped in $Fo_{90.6-92}$ have relatively low La contents and La/Yb ratios, these values are greater than zero. If the melting model is correct then this misfit between the red curve and the observed melt inclusions compositions at Fo_{90-92} indicates that the shallowest instantaneous melts were not trapped in growing olivines before mixing with other melts. The La contents of the melts

Figure 9. (opposite) Variation in elemental concentrations and principal component scores for melt inclusion and converted clinopyroxene compositions as a function of host (mi) or equilibrium (cpx) olivine composition. The principal components were calculated as described in the text and are shown in Table 4. (a) The data are shown as red circles. The running average, calculated as described in the text, is shown as a black line. The dashed blue line shows the results of the ol/cpx fractionation models described in section 4.4 and the solid blue line that of models with plagioclase crystallization included. The REEs were assumed to be perfectly incompatible ($D = 0$) during crystallization because clinopyroxene constitutes <30% of the crystallizing material (giving bulk $D < 0.15$ for all REEs) and the extent of crystallization is <40%. The black cross shows the 1σ analytical precision calculated from repeat measurements. (b) Plot of standard deviation of the element or principal component against host olivine composition. The standard deviation is shown as a thin black line and the dashed lines show the 95% confidence intervals. The standard deviation and confidence intervals were calculated as described in the text. c) Mixing parameter, M, calculated as described in the text, plotted as a function of host olivine composition.
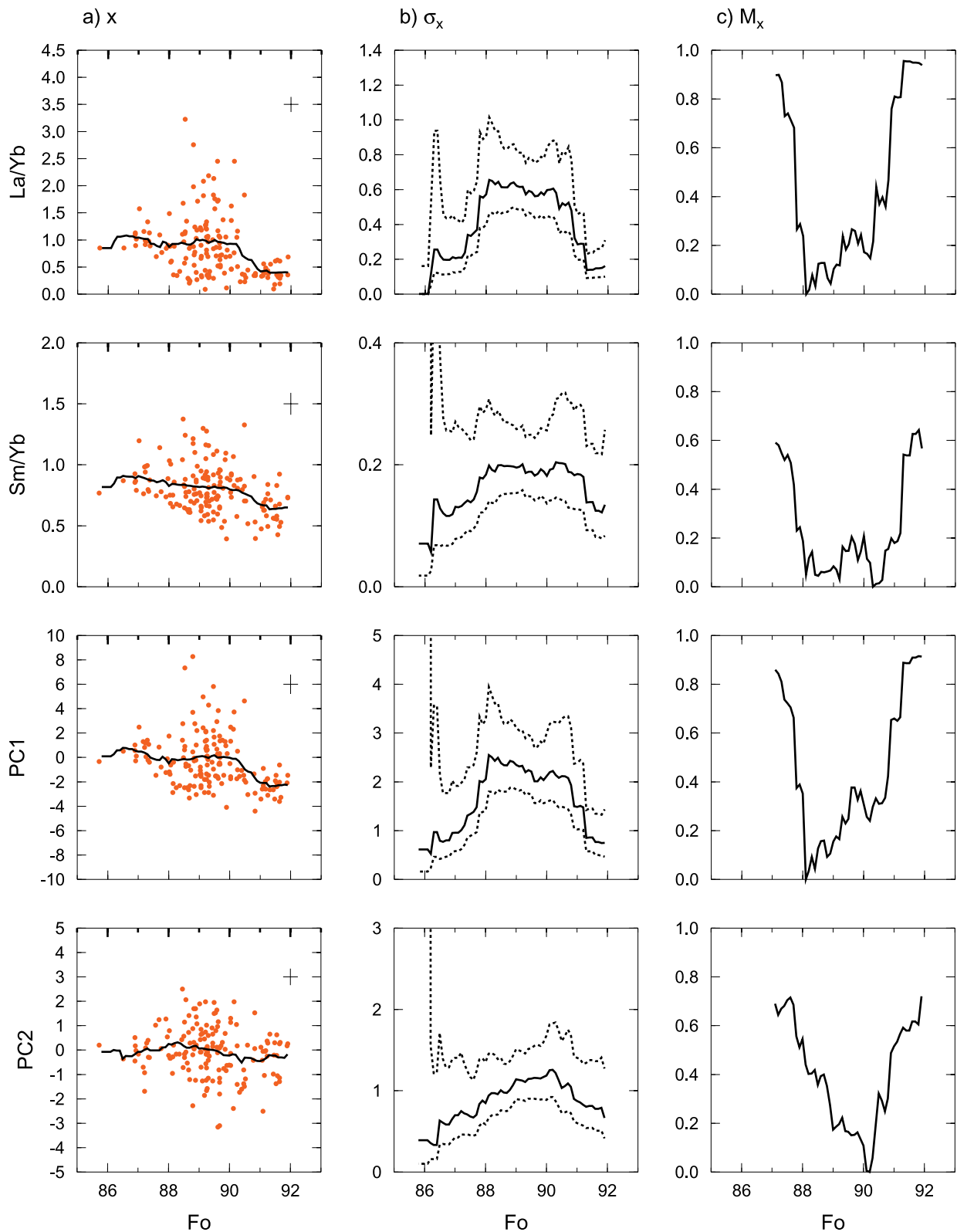
Figure 10. Same as Figure 9 but REE concentration ratios with respect to Yb are used instead of absolute concentrations. The principal components are given in Table 5.

Geochemistry
Geophysics
Geosystems
G^3

MACLENNAN ET AL.: MELT MIXING

10.1029/2003GC000558

Table 4. Principal Components for Melt Enclusion REE Concentrations

	σ	V (%)	La	Ce	Nd	Sm	Eu	Dy	Er	Yb
p_1	2.13	56.81	0.341	0.355	0.377	0.380	0.391	0.351	0.309	0.316
p_2	1.41	25.02	0.417	0.432	0.319	0.006	−0.014	−0.416	−0.402	−0.451
p_3	0.722	6.51	0.305	0.255	0.033	−0.669	−0.358	−0.014	0.501	0.118

Principal components for melt inclusion REE concentrations. The principal components were calculated from the matrix of correlation coefficients, as described in *Albarède* [1995]. The standard deviation associated with each principal component is shown as σ and the percentage of the total variance described by the principal component is *V*.

included in the most forsteritic olivines may be generated by mixing of the predicted fractional melts produced after 20–25% melting with 0.2–3.5% of the compositionally extreme melt produced at the onset of melting. This melt mixture is also predicted to be in equilibrium with Fo_{91-92} olivines, and therefore can also account for composition of the host olivines. Mixing of such extreme melts may occur if melt pathways in the mantle are able to transport deep melts to near surface regions, to prevent them mixing with melts with generated at intermediate depths, and then to bring them into contact with instantaneous melts generated at large extents of melting.

[32] Although incomplete mixing of fractional melts and fractional crystallization can account for the observed range of melt inclusion and host olivine compositions, it is likely that variation in the composition of melt generated under Theistareykir results both from melting and from variability in the composition of the mantle source [*Stracke et al.*, 2003]. Unfortunately isotopic data are not yet available for the melt inclusion compositions, so it is not possible to evaluate the relative importance of melting and source variation in the generation of their compositional range.

4.4. Crystallization and Cooling

[33] In order to compare the geochemical observations with the results of physical models of mag-

matic behavior it is desirable to convert the compositional variation into estimates of variation in degree of crystallization, temperature and extent of mixing. The extent of crystallization was calculated using the variation in the forsterite content of the host olivine. If the variation in Mg# of the melt, and hence the forsterite content of the crystallizing olivine, is caused by crystallization of phases such as olivine or clinopyroxene with $K_d^{Fe\text{-}Mg} \sim 0.3$ then the degree of crystallization, *F*, required to change the olivine composition from Fo_i to Fo_f can be estimated using a modified version of the approach described by *Albarède* [1995]. By rearrangement of his equations 1.5.19 and 1.5.20 the fraction crystallized, *F*, can be obtained from

$$F = 1 - \left[\frac{Mg_i}{Mg_f} \left(\frac{Fe_f}{Mg_f} \frac{Mg_i}{Fe_i} \right)^{\frac{1}{K_d - 1}} \right] \quad (1)$$

where Mg_i and Mg_f are respectively the initial and final Mg contents of the melt, and Fe_i and Fe_f are the iron contents. The Fe/Mg ratio in the melt is related to the olivine compositions by K_d with

$$\frac{Fe^{2+}}{Mg} = \frac{1}{K_d} \left(\frac{1 - Fo}{Fo} \right) \quad (2)$$

where in this case Fo is the mole fraction of forsterite in the olivine and Fe^{2+} and Mg are mole fractions in the melt. The partitioning of Mg

Table 5. Principal Components for Melt Inclusion REE/Yb Ratios

	σ	V (%)	La	Ce	Nd	Sm	Eu	Dy	Er
p_1	2.02	58.48	0.426	0.449	0.442	0.384	0.371	0.283	0.237
p_2	1.09	16.99	0.334	0.304	0.236	−0.060	−0.127	−0.625	−0.574
p_3	0.845	10.21	0.210	0.201	0.137	−0.401	−0.497	−0.210	0.666

Same as Table 4 but using REE/Yb ratios.

Table 6. Precision Estimates for EMP Analyses

	Cpx			Ol		
	$\bar{x}$	σ_r	P	$\bar{x}$	σ_r	P
SiO$_2$	51.24	0.18	0.34	40.58	0.27	0.66
TiO$_2$	0.19	0.03	15.21	-	-	-
Al$_2$O$_3$	5.38	0.09	1.62	-	-	-
Cr$_2$O$_3$	1.29	0.05	3.55	-	-	-
FeO	3.92	0.07	1.69	11.05	0.21	1.93
MnO	0.12	0.05	36.75	0.18	0.04	20.34
MgO	16.81	0.09	0.51	46.70	0.30	0.64
CaO	20.73	0.06	0.28	0.35	0.01	3.64
Na$_2$O	0.26	0.01	3.98	-	-	-
NiO	0.05	0.01	23.63	0.28	0.01	4.44
Mg#	88.43	0.17	0.19	88.29	0.24	0.27

Precision estimates for EMP analyses from 20 closely spaced (within 100 μm) repeat measurements on clinopyroxene and olivine crystals. The average of the repeats is given by $\bar{x}$ and the standard deviation of the repeats is given by σ_r. The mean and standard deviation are given in wt%. The precision, P, is given as percent relative by $100 \times \sigma_r/\bar{x}$.

between melt and olivine was modelled using the expression of *Beattie* [1993]

$$D_{Mg} = \frac{0.667 - 0.031\text{Fe}}{0.279\text{Fe} + \text{Mg}} \qquad (3)$$

with D_{Mg} being the partition coefficient. The Ds and equilibrium olivine composition were calculated for Theistareykir whole-rock samples in the compositional range of interest using Equation 3 for the D calculations and $K_d = 0.3$ and melt Fe^{2+}/Fe = 0.9 for the olivine calculations. As expected the calculated olivine compositions and Ds show a strong correlation ($r = -0.91$) with

$$D_{Mg} = 25.5 - 25\text{Fo} \qquad (4)$$

being the best fitting straight line. The MgO content (wt%) of olivine can be calculated from its Fo content using the stoichiometry of olivines in the forsterite-fayalite solid solution

$$\text{MgO}_{ol} = \frac{70.52\text{Fo}}{1.78 - 0.553\text{Fo}}. \qquad (5)$$

Equation 1 can then be expressed in terms of initial, Fo$_i$, and final, Fo$_f$, olivine compositions using Equations 2, 4 and 5 and by simplifying as

$$F = 1 - \left(\frac{1 - 0.98\text{Fo}_f}{1 - 0.98\text{Fo}_i}\right)\left(\frac{\text{Fo}_i}{1 - 0.31\text{Fo}_i}\right)\left(\frac{1 - 0.31\text{Fo}_f}{\text{Fo}_f}\right)$$
$$\cdot \left[\left(\frac{\text{Fo}_i}{1 - \text{Fo}_i}\right)\left(\frac{1 - \text{Fo}_f}{\text{Fo}_f}\right)\right]^{\frac{1}{K_d - 1}} \qquad (6)$$

[34] The relationship between degree of crystallization and olivine composition calculated using Equation 6 is shown for two starting compositions in Figure 12. If plagioclase is present in the crystallizing assemblage then the values obtained from Equation 6 will be underestimates. The point counting results from Table 1 show that in nodules which have average olivine with a forsterite content of less than 88.5 mol%, plagioclase constitutes ∼50% of the crystallizing assemblage. Fractionation models which correct for the effect of this plagioclase crystallization are also shown in Figure 12.

[35] Estimates in the variation in temperature can be obtained using the olivine-melt thermometer of *Roeder and Emslie* [1970] which uses the molar MgO contents of equilibrium olivine, X_{MgO}^{ol}, and melt, X_{MgO}^l. If the forsterite content of the olivine is known then X_{MgO}^{ol} can be determined directly from the olivine stoichiometry. The X_{MgO}^l were estimated as follows. The equilbrium melt Mg# for a given forsterite content was calculated assuming $K_d^{Fe-Mg} = 0.3$ and that 90% of the total Fe is present as Fe^{2+}. Then the molar MgO content of the equilibrium melt was determined using the relationship

$$X_{MgO}^l = 0.02 + 0.0083 \exp(4.2\text{Mg\#}^l), \qquad (7)$$

which was calculated using the Theistareykir whole-rock compositions which have Mg#s between 60 and 80 [*Slater et al.*, 2001; *Maclennan et al.*, 2002; *Maclennan et al.*, 2003]. While this relationship gives a correlation coefficient of 0.96 for the whole-rock compositions, Figure 8 shows

Table 7. Precision Estimates for SIMS Analyses

	MIs			Cpx		
	$\bar{x}$	σ_r	P	$\bar{x}$	σ_r	P
La	1.66	0.23	13.94	0.06	0.01	6.66
Ce	4.37	0.55	12.56	0.27	0.02	9.25
Nd	3.42	0.44	12.74	0.43	0.03	7.26
Sm	1.39	0.18	12.65	0.29	0.03	11.27
Eu	0.70	0.10	14.48	0.13	0.01	9.67
Dy	2.22	0.17	7.76	0.75	0.07	8.76
Er	1.44	0.10	6.69	0.47	0.04	9.20
Yb	1.54	0.08	5.12	0.48	0.04	9.04

Precision estimates for SIMS analyses. The melt inclusion precision is based on 16 repeat analyses and that for the clinopyroxene is based on 15 repeats. The mean and standard deviation are given in ppm.

a)

b)
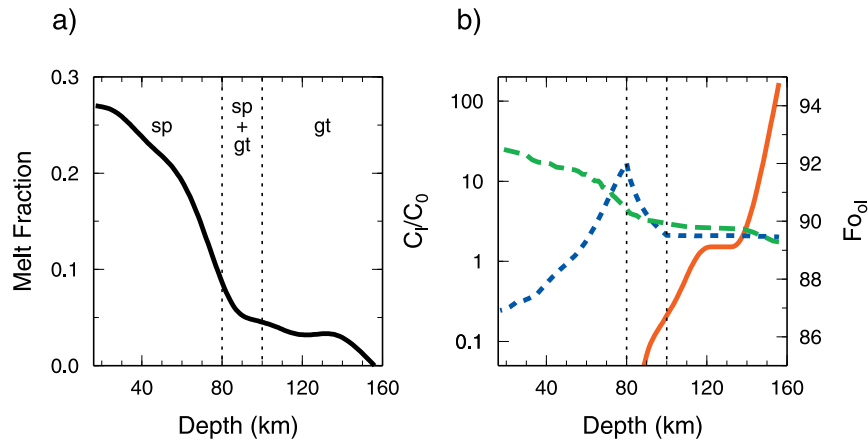
Figure 11. (a) Best fitting melt fraction against depth model for Theistareykir [*Maclennan et al.*, 2003]. The dashed lines mark the depths of the spinel-garnet transition. (b) Predicted instantaneous fractional melt compositions from the model in Figure 11a. The La and Yb concentrations are shown normalized to the mantle source composition (left axis). La is shown as a solid red line and Yb as a short-dashed blue line. The green long-dashed line shows the calculated forsterite content of the olivine in equilibrium with the fractional melts.

that variation in the trace element composition of the melt inclusions is different to that found in the whole-rock, so the relationship between X^l_{MgO} and Mg#[l] for melt inclusions and whole-rock samples may also differ. Unfortunately, the original relationship between X_{MgO} and Mg# in the melt inclusions is likely to have been obscured by post-entrapment processes [*Gaetani and Watson*, 2000]. Crystallization temperatures estimated from olivine compositions are shown in Figure 12.

[36] The degree of crystallization estimates and temperature evolution calculated as described above are compared with a high pressure fractional crystallization model of *Weaver and Langmuir* [1990] in Figure 12. The relationships between F and Fo are in broad agreement, with both predicting an interval of ~25% crystallization between Fo_{90} and Fo_{86}. While the predicted temperatures from the two methods agree to within ±10°C between Fo_{91} and Fo_{87}, the gradient, dT/dF, from the *Roeder and Emslie* [1970] estimate is steeper than that from the *Weaver and Langmuir* [1990] models. Furthermore, the *Weaver and Langmuir* [1990] model has a large change in gradient at the onset of plagioclase crystallization, which is not present in the *Roeder and Emslie* [1970] estimate. This feature, which corresponds to an increase in dF/dT when plagioclase joins the crystallising assemblage, is common in fractional crystallization

models for compositions similar to primitive MORB [*Kelemen and Aharonov*, 1998].

[37] Inspection of Figures 9 and 10 shows that concentrations and light REE/Yb concentration ratios are low in melt inclusions that are hosted in olivines with forsterite contents of greater than 90.6. At forsterite contents lower than this value the mean concentration of all of the melt inclusion REEs increases with decreasing forsterite content and the mean concentration ratios remain almost constant (e.g., La/Yb$_{av}$ = 0.96 ± 0.07 between $Fo_{90.6}$ and Fo_{85}). Increases in REE concentrations with decreasing olivine forsterite content can be calculated directly from the degree of crystallization estimates shown in Figure 12. The estimated increase in La, Sm and Yb contents for these models are plotted in Figure 9 and the predicted fractionation paths including plagioclase lie within the range of observed REE contents and within ~10% of the running averages of these observations at Fo > 87 mol%. Therefore the variation in REE concentration and ratios in the melt inclusions with decreasing forsterite content is consistent with the gradual mixing of variable mantle melts as fractional crystallization proceeds. More complicated crystallization models such as RTF [*O'Hara and Mathews*, 1981] or in situ [*Langmuir*, 1989] are not required to account for the observations. Furthermore, the near constant average values of

a)

b)
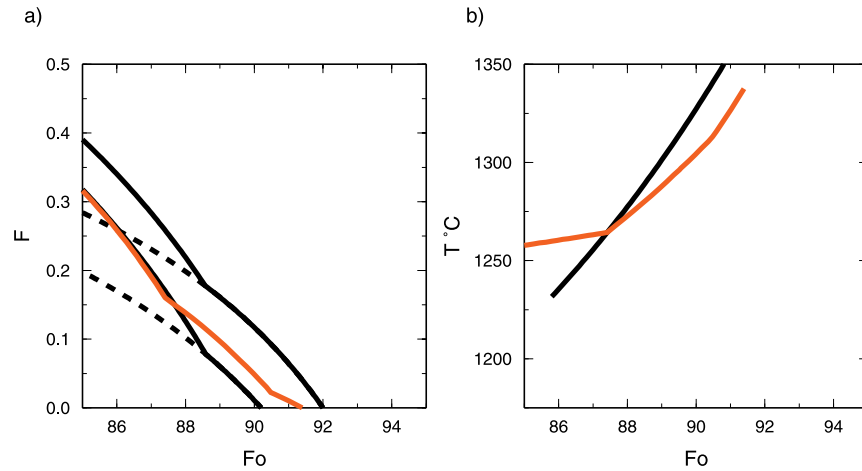
Figure 12. (a) Black lines show the relationship between fraction crystallized, F, and the forsterite content of the equilibrium olivine for two different starting compositions. The dashed black lines show the predicted F for crystallization of phases with $K_d \sim 0.3$ only (olivine, clinopyroxene) and were calculated using Equation 6. The solid line shows the predicted F if 50% of the crystallizing assemblage consists of plagioclase at forsterite contents of less than 88.6 mol%. The red line shows the relationship between F and Fo obtained using the model of *Weaver and Langmuir* [1990] with the average Borgarhraun melt as a starting composition [*Maclennan et al.*, 2003], a pressure of 0.8 GPa and an oxygen fugacity held at one log unit beneath the quartz-fayalite-magnetite buffer. (b) The black solid line is the relationship between temperature and Fo for Borgarhraun samples calculated using the thermometer of *Roeder and Emslie* [1970] as described in the text. The red line shows the relationship for the *Weaver and Langmuir* [1990] fractionation model detailed in Figure 12a.

REE/Yb ratios, the decrease in the maximum values of La/Yb and the decrease in the variability of La/Yb with decreasing forsterite content indicate that variation in incompatible trace element ratios is not caused by crystallization processes.

4.5. Melt Mixing

[38] The evolution in average REE concentration in the melt inclusions as a function of the host olivine composition is accompanied by changes in the variability of the melt inclusion composition (Figures 9 and 10). This evolution in variability provides a record of melt mixing, and can be quantified by calculating the standard deviation of the melt inclusion compositions as a function of host olivine composition. The black lines in column (a) of Figure 9 and Figure 10 show the running average of the melt inclusion compositions, calculated at the mid-point of a box with a width of 1.5 Fo units. The standard deviation of the melt inclusion compositions was calculated for the same box width, and is shown in column (b) of Figures 9 and 10. The uncertainty in the estimate of standard deviation is controlled by the number

of samples used in the estimate so that the greater the number of samples used to calculate the standard deviation, the smaller the uncertainty in the estimate. The 95% confidence interval for the standard deviation was calculated using the χ^2 distribution, and this interval is shown in dashed lines on Figures 9 and 10. The estimates of standard deviation are reliable between Fo$_{87}$ and Fo$_{92}$; outside this range there are too few samples in each box to provide good estimates of the standard deviation. A useful measure of the degree of mixing is the parameter defined by

$$M = 1 - \frac{\sigma_o^2}{\sigma_m^2} \qquad (8)$$

where σ_o is the observed standard deviation in melt inclusion composition at a given olivine content and σ_m is the maximum standard deviation. This parameter simply reflects changes in the variance of a given element or ratio compared to its maximum variance. Therefore M is sensitive both to the generation of geochemical variation during melting or crystallization and to its destruction during melt mixing. Mixing causes M to increase,

while the generation of variability causes M to decrease. One advantage of using M to study mixing is that it can only take values between 0 and 1, and therefore provides a useful means for comparing the behavior of different elements or element ratios.

[39] The evolution of M with forsterite content of the host olivine is shown in column (c) of Figures 9 and 10. The M evolution calculated for REE concentrations, ratios and principal components share a number of common features. The value of M drops between Fo_{92} and Fo_{91}, and is close to its lowest values ($M < 0.2$) between Fo_{91} and Fo_{90}. This drop in M may reflect the initial establishment of the compositional variability by fractional melts of the mantle. The results of the melting model shown in Figure 11 demonstrate that the mantle melts in equilibrium with the most forsteritic olivines (Fo_{92}) have a limited range of low REE contents. If these melts lose about 5% of their mass through crystallization then their REE contents will be little changed, but they will be in equilibrium with Fo_{90-91} olivines. Predicted fractional melt compositions from the initial stages of melting are also in equilibrium with Fo_{90-91} olivines, but have far higher REE contents than the mantle melts that were originally in equilibrium with Fo_{92} olivines. The model prediction is therefore that melt inclusions with low REE contents may be in equilibrium with both Fo_{92} and $Fo_{<91}$ olivines while melts with high REE contents are only in equilibrium with $Fo_{<91}$ olivines. Supply of incompletely mixed fractional melts of the mantle, coupled with crystallization, therefore provides a means of accounting for the increase in variability, or decrease in M, between Fo_{92} and Fo_{90-91}.

[40] At lower forsterite contents a different relationship between host olivine compositions and melt inclusion REE variation is recorded by M. Between Fo_{90} and Fo_{87} M increases toward an average value of 0.71 ± 0.08 for REE concentrations and 0.80 ± 0.11 for REE/Yb ratios. While the decreases in M between Fo_{92} and Fo_{91} reflect the initial establishment of the variability from fractional melts, the large increases between Fo_{90} and Fo_{87} record concurrent mixing and crystallization. The value of M increases toward one as mixing

destroys the compositional variability, and the Fo content of the olivines drops as crystallization progresses.

[41] The relative rates of mixing and crystallization can be estimated from the increases in M between Fo_{90} and Fo_{87}. The average dM/dFo in this crystallization interval is -0.12 ± 0.06 for REE concentrations and -0.20 ± 0.03 for REE/Yb ratios. The estimated mixing rates for the ratios are higher than those for the concentrations because at low Fo contents fractional crystallization generates no variation in REE ratios, but produces variation in absolute concentrations. Using the relationships between the olivine composition, degree of crystallization and temperature shown in Figure 12, these relative rates correspond to dM/dF of 1.69 and 2.76 and dM/dT of -0.46×10^{-3} °C^{-1} and -0.76×10^{-3} °C^{-1}.

[42] While these estimates of the relative rates of mixing and crystallization may provide useful constraints upon the physics of magma storage under Theistareykir, systematic differences in the evolution of M with olivine host composition between heavy and light REEs cannot be accounted for by mixing and crystallization alone. These differences are illustrated in Figure 13a, using M calculated for La and Yb concentrations as examples. While both elements reach their lowest M between Fo_{91} and Fo_{90} and have $M \sim 0.8$ at Fo_{87}, the evolution of M between Fo_{90} and Fo_{87} is quite different for the two elements. For instance, at $Fo_{88.5}$, La has $M \sim 0.1$ while Yb has $M \sim 0.7$. So between Fo_{90} and Fo_{88}, where Yb variation is strongly reduced, La variability is maintained. If mixing and crystallization alone controlled the evolution of M then both La and Yb should exhibit similar variation in M with decreasing Fo. While the behavior of Yb between Fo_{90} and Fo_{88} indicates that melt mixing is taking place in this interval, the low M for La indicates that La variability is being generated as rapidly as it is being destroyed by mixing. Inspection of Figures 9 and 10 shows that the process that generates variability in La (and La/Yb) between Fo_{90} and Fo_{88} must preserve the average La/Yb ratio and average La and Yb concentrations and must not generate strong variability in Yb.
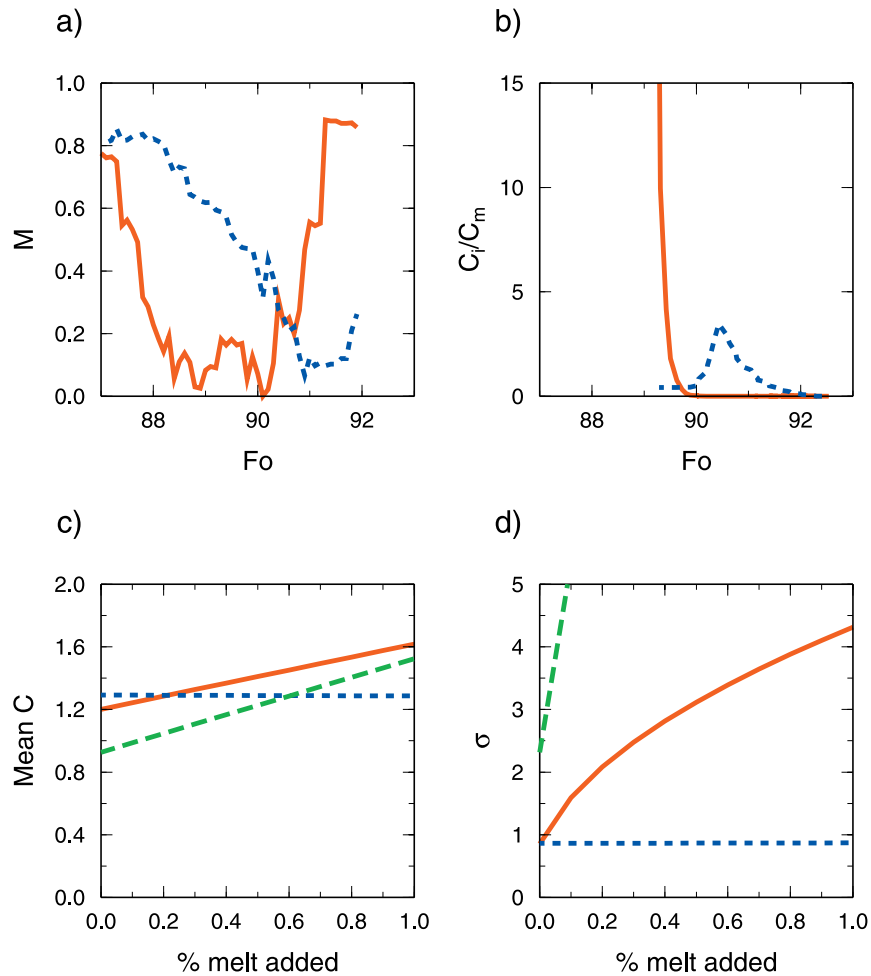
Figure 13. (a) Comparison of observed M for La (solid red line) and Yb (dotted blue line). (b) Predicted composition of instantaneous fractional melts from Theistareykir melting model (See Figure 11). The instantaneous compositions, C_i are shown here normalized to the mean predicted melt composition, C_m, from the melting model. The solid red line is La and the dotted blue one is Yb. (c) Variation in average composition caused by addition of extreme initial melts from the melting model to the distribution of melt inclusion compositions found at Fo_{90}. This variation was calculated using equation (9). The La concentration (ppm) is shown in a solid red line, the Yb concentration (ppm) in a dotted blue line and the La/Yb ratio in a green dashed line. (d) Variation in standard deviation of the sample caused by introduction of extreme initial melts to the distribution of melt inclusion compositions found at Fo_{90}. This variation was calculated using equation (10). The lines have the same colors as those used in Figure 13c.

[43] Figure 11b shows that instantaneous fractional melts generated at the onset of melting in the garnet field have extremely high La contents, about 20 times higher than those of the average melt generated by the model, while the Yb contents of the initial melts are similar to those of the average model melt. The cause of this difference in relative concentration is that the onset of melting takes place in the garnet stability field, where La is highly incompatible, but Yb has a bulk partition coefficient of close to 1. In contrast, Yb becomes incompatible

once garnet breaks down to form spinel at depths of 80–100 km and the Yb concentration of the melts formed at this depth is up to 4 times higher than that of the average melt. The predicted MgO and FeO content of the fractional melts also changes with depth, and this change is mirrored by variation in the calculated composition of olivines in equilibrium with the melts (Figure 11b). While the initial melts are in equilibrium with Fo_{89} olivines, the shallowest melts would crystallize Fo_{92} olivines. The relationship between the melt La and Yb contents and the

predicted equilibrium olivine composition is shown in Figure 13b. The full range of Yb contents is found in melts that are in equilibrium with Fo_{90-91} olivines but the maximum variability in La contents is found in melts in equilibrium with Fo_{89}. This difference in the Fo content of olivines in equilibrium with melts with the highest La and Yb may account for the observed difference in mixing behavior with host olivine Fo content (Figure 13a). Fractional melts in equilibrium with Fo_{90-92} olivines show the maximum variability in Yb contents, but very little variation in La. Concurrent mixing and crystallization of these melts will reduce the Yb variability by mixing and the Fo content of the host olivine through crystallization. This mixing and crystallization can account for the mixing behavior of Yb between Fo_{91} and Fo_{88}. However, the presence of fractional melts that have extremely high La contents and are in equilibrium with Fo_{89-90} olivines provides La variability that balances the mixing between Fo_{90} and Fo_{88}.

[44] The influence of addition of these extreme melts to the distribution of Borgarhraun melt inclusion compositions was investigated using a simple approach where extreme, unmixed melt compositions were introduced to the distribution of melt inclusion compositions observed in the box centered at Fo_{90}. If it is assumed that each of the N melt inclusion measurements represents an equal mass of melt then the addition of extreme melts with a mass fraction f_e of the original mass gives the following expression for the mean of the new distribution

$$\bar{x}_f = \frac{\bar{x}_0 + f_e x_e}{1 + f_e} \tag{9}$$

where $\bar{x}_0$ was the mean of the original distribution and x_e is the composition of the extreme melt. If the changes in the mean are small then the variance of the new distribution is

$$\sigma_f^2 \approx \frac{\sigma_0^2(N-1) + f_e N(x_e - \bar{x}_0)^2}{N + f_e N - 1} \tag{10}$$

where σ_0^2 is the variance of the original distribution. Figures 13c and 13d show that addition of small fractions of the initial mantle melts to the distribution of melt inclusion compositions found

in the box centered at Fo_{90} can generate large increases in the standard deviation in La and La/Yb while having little effect on the standard deviation of Yb or the mean compositions of La, Yb or La/Yb. Addition of <0.1% of such melts to the magma body can account for the balance between mixing and generation of variation observed in La between Fo_{90} and Fo_{88} and the domination of mixing observed in Yb over the same interval.

5. Oxygen Isotopes

5.1. Models of the Generation of Oxygen Isotope Variability

[45] Oxygen isotope variation in Icelandic basalts and picrites has received much attention in the last 10 years [Nicholson et al., 1991; Hémond et al., 1993; Eiler et al., 2000; Skovgaard et al., 2001] but there has been limited agreement on the principal cause of this variation. Nicholson et al. [1991] and Eiler et al. [2000] have presented oxygen isotope measurements from the full range of erupted rock types at Theistareykir and the neighbouring Krafla system. While the most primitive Theistareykir picrites have relatively high $\delta^{18}O_{ol}$ of 4–5 per. mil., the Krafla rhyolites have $\delta^{18}O_{ol}$ of 0–2 per. mil. with a broad positive correlation between the MgO content and $\delta^{18}O$ of the sample. This correlation may be successfully reproduced by a crustal assimilation-fractional crystallization (AFC) model [Nicholson et al., 1991; Eiler et al., 2000]. Hydrothermal fluids in Iceland have $\delta^{18}O$ of as low as −11 [Sveinbjörnsdóttir et al., 1986] so hydrothermally altered crust is also likely to have low $\delta^{18}O$ [Gautason and Muehlenbachs, 1998]. Coupled crystallization of basalt with assimilation of low $\delta^{18}O$ crustal material generates a correlation between melt Mg# and $\delta^{18}O$. Nicholson et al. [1991] proposed that the assimilated material was rhyolite produced by remelting of the hydrothermally altered crust, and had a $\delta^{18}O$ of 0–2, a Mg# of 10 and a La content of ~45 ppm. Eiler et al. [2000] also favored a low Mg# assimilant, an andesite with $\delta^{18}O \sim 0$, Mg#~30 and La ~30 ppm. Since the primitive Theistareykir basalts have high $\delta^{18}O$, high Mg# (~70) and low La contents (<1 ppm), an AFC process involving either of these assimilants

will produce correlations between Mg#, La concentrations and $\delta^{18}O$.

[46] While there is strong evidence that crustal processes control the oxygen isotope characteristics of the evolved rocks at Krafla and Theistareykir, a number of authors have suggested that oxygen isotope variation in primitive Icelandic basalts and picrites reflects variation in the composition of melts that were supplied to the crust, and therefore variation in the oxygen isotope composition of the mantle under Iceland [*Skovgaard et al.*, 2001; *Gurenko and Chaussidon*, 2002]. Melts of peridotite mantle or peridotite/basalt mixtures are predicted to have high Mg# and, for example, *Kogiso et al.* [1998] found that melts of mixture KG2, made of 33% MORB and 67% peridotite KLB-1, have Mg#s between 67 and 75. Therefore if oxygen isotope variability is present in mantle melts, the relationship between $\delta^{18}O$ and Mg# will be quite different to that produced by AFC processes. A large range in $\delta^{18}O$ would be expected for little variation in the Mg# of the melt. Trace element and radiogenic isotope variability is known to be present in mantle melts supplied to Theistareykir [*Slater et al.*, 2001; *Maclennan et al.*, 2002; *Stracke et al.*, 2003], so if oxygen isotope variability is also present in mantle melts the mixing behavior of oxygen isotopes may be similar to that observed for the REEs in Borgarhraun melt inclusions.

5.2. Correlations Within Theistareykir Whole-Rock Samples

[47] The oxygen isotope measurements of *Eiler et al.* [2000] were made on crystal separates, and in order to relate these measurements to the major and trace element composition of the whole-rock samples it was necessary to assume that the crystals from individual specimens were in oxygen isotopic equilibrium with the specimen. However, such oxygen isotope equilibrium is not present within individual samples because *Eiler et al.* [2000] reported oxygen isotope variability of up to 0.7 per. mil. in olivine crystals from single specimens, greater than the entire range of isotopic variability found in the sample averages. Nonetheless, *Eiler et al.* [2000] observed correlations between both the average oxygen isotope composition of crystals

from specimens and the trace element (e.g., La/Yb) and major element (e.g., Mg#) compositions of these specimens. The relationships between whole-rock La/Yb and Mg# and the $\delta^{18}O$ of individual crystals or sample averages are shown in Figure 14. While the low MgO rocks from Krafla and Theistareykir are influenced by crustal processes, the cause of oxygen isotope variability in the most mafic Theistareykir basalts and picrites is not unambiguously resolved by the data shown in Figure 14 [*Eiler et al.*, 2000]. The data in Figures 14c and 14d show that the correlation between $\delta^{18}O$ and whole-rock La/Yb is far stronger than that of $\delta^{18}O$ and Mg#.

5.3. Correlations With Crystal and Melt Inclusion Compositions

[48] While the data of *Eiler et al.* [2000] show that there is a large variability in the oxygen isotope composition of olivines found in melts that have similar Mg#s to those expected for mantle melts, the lack of equilibrium between the olivines and their host samples introduces uncertainty into the interpretation of the data. For instance, the individual olivine $\delta^{18}O$ of ~4.13 per. mil. measured in a Borgarhraun sample with a calculated melt Mg# of 69 (Figure 14a) may have crystallised from more evolved lava that has assimilated crustal material and then been incorporated in the Borgrahraun melt during its ascent to the surface. Such uncertainty can be minimized by measuring the major and trace element compositions of the crystals and melt inclusions of the same crystals that are to be analyzed for $\delta^{18}O$. Therefore the oxygen isotope composition of Borgarhraun crystals which had been analyzed for major and trace element compositions are shown in Figure 15. The red and green symbols in Figure 15 show measurements from a single crystal, so that the composition of the crystals and melt inclusions were determined by electron and ion-probe before $\delta^{18}O$ was measured on the same crystal. Such measurements give the strongest available constraints on the relationship between major or trace element concentrations and oxygen isotope compositions. Some of the crystals that had been probed for majors and traces were not large enough for oxygen isotope analysis, and for these cases a composite sample was created for
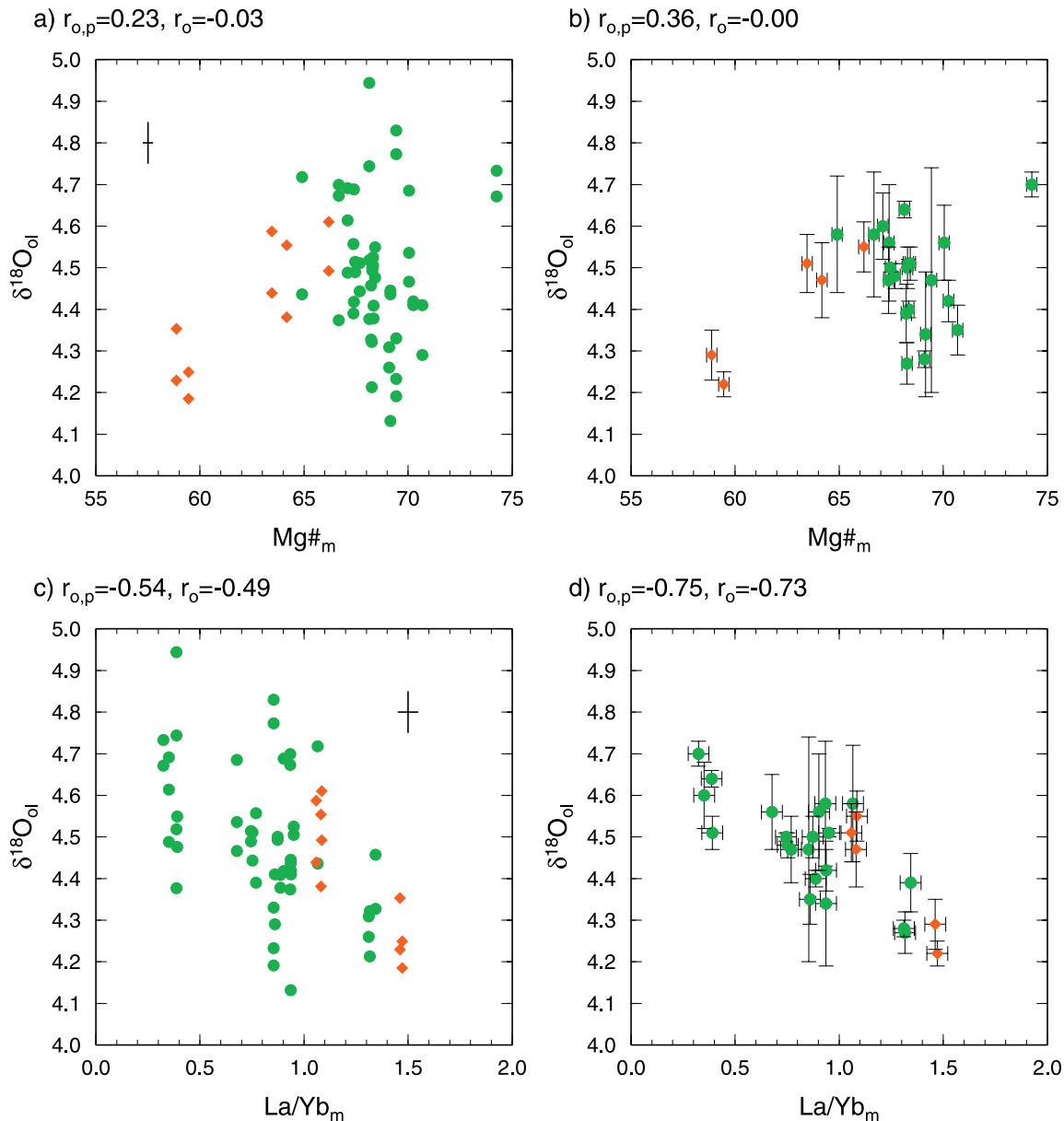
Figure 14. Oxygen isotope data from *Eiler et al.* [2000]. Figures 14a and 14c show the $\delta^{18}O$ of individual crystals plotted against their host sample composition, while Figures 14b and 14d show the average $\delta^{18}O$ of crystals in a sample plotted against the sample composition. The green circles show $\delta^{18}O_{ol}$ measurements that were made on olivine crystals. The red diamonds show $\delta^{18}O_{ol}$ predicted from $\delta^{18}O$ on plagioclase using the high-temperature fractionation of $\sim$0.6 per. mil. from *Chiba et al.* [1989]. The error bars in Figures 14a and 14c show the 1σ precision error for each point, while those for $\delta^{18}O_{ol}$ in Figures 14b and 14d are the 1σ variability of the measurements in each sample. The Mg# of the melt was taken from the calculation of *Eiler et al.* [2000], who corrected the composition of each sample for the effect of olivine accumulation. The correlation coefficients are shown both for the entire data-set, $r_{o,p}$, and for the measurements made on olivine crystals alone, r_o.

oxygen isotope analysis by placing a number of crystals from the same nodule within the sample holder. The individual nodules are not in internal oxygen isotope equilibrium (section 3.2) so these composites, shown as blue on Figure 15, may suffer from some of the same disequilibrium problems as those for the whole rock/crystal pairs of *Eiler et al.* [2000].
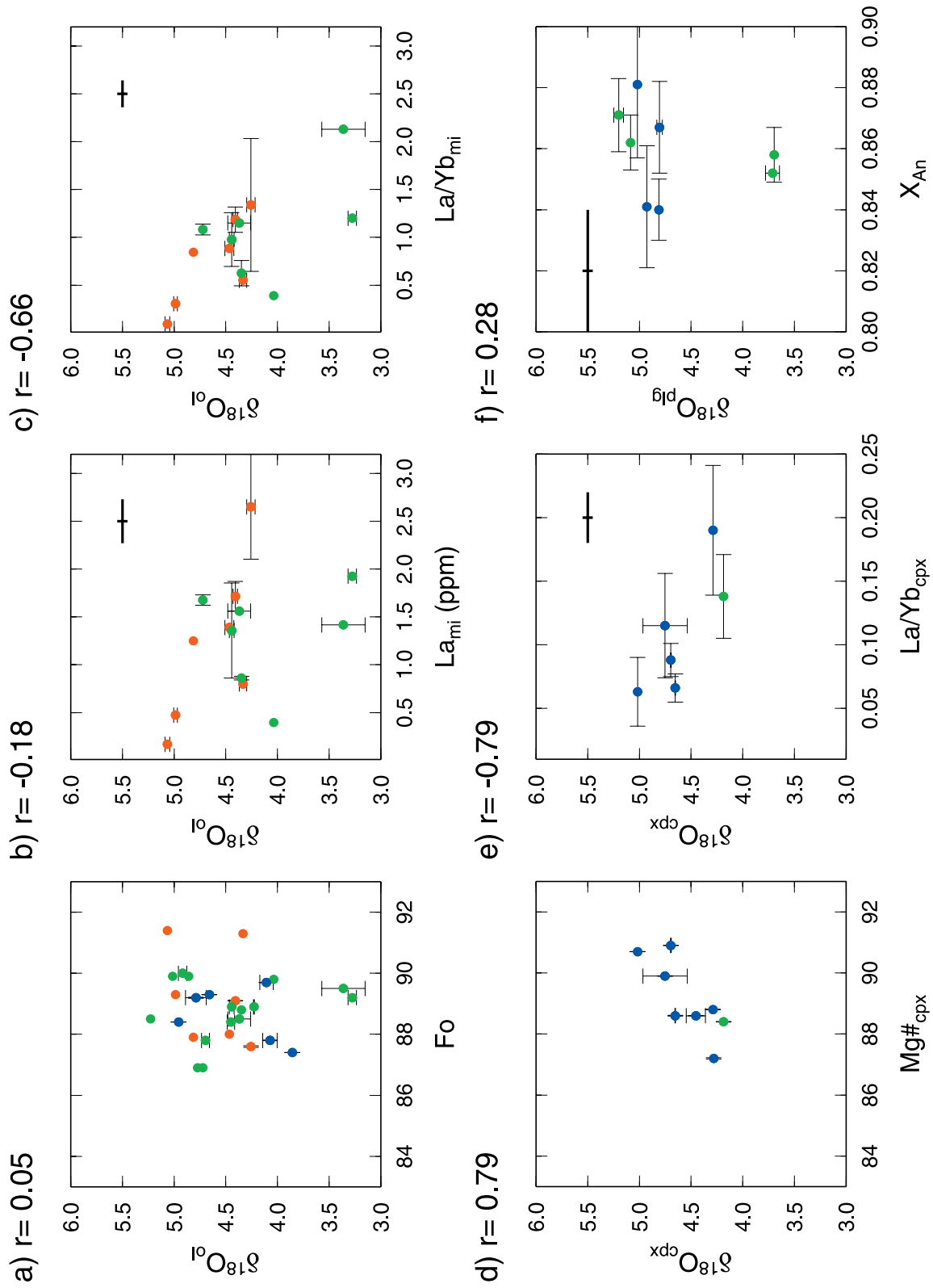
[49] The observed $\delta^{18}O$ of Borgarhraun phenocryst and nodule olivine is even more variable than those reported by *Eiler et al.* [2000], ranging from 3.3 to 5.2 per. mil.. This variation shows no correlation with the major element composition of the olivine, and the full range of $\delta^{18}O$ variability is found in olivines that have forsterite contents between 88 and 90 mol%. These olivines have compositions that are in equilibrium with mantle melts and also contain melt inclusions that exhibit the maximum variability in REE contents and REE/Yb ratios (section 4). The correlation between the oxygen isotope composition of the host olivine and the La content of the melt inclusions is poor, but La/Yb has the strongest correlation of any geochemical indicator from the olivines or melt inclusions with the host olivine $\delta^{18}O$. The available clinopyroxene data show strong correlations between clinopyroxene Mg# or La/Yb and the $\delta^{18}O$. The Mg#-$\delta^{18}O$ relationships for the olivines and clinopyroxenes are therefore different, which presents problems for straightforward interpretation of the data. While the strong correlation observed in the clinopyroxene compositions is evidence in support of an AFC origin for the oxygen isotope variability, the lack of correlation for olivine compositions is consistent with a mantle source origin for this variability. In the following few paragraphs two possible explanations for the apparent conflict between the olivine and clinpyroxene data are investigated, one which involves disruption of the olivine forsterite contents by diffusion, and another which is based upon differences in the nature and quantity of data.

[50] The Mg#-$\delta^{18}O$ correlation for clinopyroxene can be accounted for by variable amounts of assimilation of a low Mg#, low $\delta^{18}O$ material. However, such assimilation should also generate a correlation between olivine forsterite content and $\delta^{18}O$, which is not observed. One possible explanation for the poor correlation between Fo and $\delta^{18}O_{ol}$ is that such a correlation initially existed for the olivines, but was disturbed by diffusion after crystallization. Diffusive equilibration with high Mg# melts, such as Borgarhraun, alters the Fo content of olivines without affecting the Mg# of clinopyroxenes, or the oxygen isotope ratios of olivines or clinopyroxenes. Such selective equilibration may occur due to the speed of Mg-Fe diffusion in olivine compared to that in clinopyroxene, or for oxygen isotopes in either phase (see Table 2). While diffusive equilibration of Mg-Fe in an olivine with a radius of 1 mm takes about 300 years, equilibration of oxygen isotopes for the same olivine may take hundreds of thousands of years.

[51] However, the principal problem with this explanation is that a number of observations indicate that diffusive equilibration does not strongly influence the forsterite content of the Borgarhraun olivines. The first is that Mg-Fe diffusion would destroy the relationship between the REE variability of melt inclusions and the forsterite content of their host olivine (Figures 8, 9, and 10). The second is that the distribution of Mg# in clinopyroxene and Fo in olivine are similar, both ranging from ~85 to 92 (Figures 4 and 5) and with a mean Mg# of clinopyroxene of 88.7 ± 2.4 (1σ) and a mean Fo of 88.1 ± 2.5. If the Fo contents of phenocryst and nodule olivines were controlled by diffusion whereas the Mg#s of clinopyroxenes were largely undisturbed by diffusion after assimilation, then the spread, mean and standard deviation of the forsterite content of olivine and the Mg# of clinopyroxene would be expected to be different. The third piece of evidence is that the compositional trends present in the melt inclusions are different to those that are present in the Theistareykir postglacial whole rock samples, and *Eiler et al.* [2000] highlighted this difference using La/Sm and CaO/Na$_2$O systematics. The reason why this

Figure 15. (opposite) Summary of oxygen isotope measurements on olivine, clinopyroxene and plagioclase crystals from Borgarhraun nodules and phenocrysts. The red circles show measurements from individual phenocrysts, and the green circles show measurements from individual crystals picked from the nodules. When elemental concentrations and oxygen isotope ratios were not available from the same crystals in nodules, the averages of all available measurements from individual nodules were taken, and these composite measurements are shown in blue circles. The error bars show one standard deviation, and where only one measurement was available no error bars are shown. The cross shown without a circle gives the 1σ analytical precision.

difference is important is that the AFC models of *Eiler et al.* [2000] were developed to account for both $\delta^{18}O$ and trace element variation in the whole rock samples. Therefore entrapment of melt with the compositional range of the whole rock samples in low Fo olivines followed by diffusion cannot account for observed relationships between olivine Fo content, oxygen isotope ratio and melt inclusion compositions. These pieces of evidence indicate that diffusion is not important in controlling the fosterite contents of Borgarhraun olivines. However, it is not possible to rule out the influence of diffusion on individual phenocrysts from the data set and more $\delta^{18}O$ data are needed to address this problem. If a systematic relationship between $\delta^{18}O_{ol}$ variation and Fo is observed, such as that for melt inclusion REE contents and the Fo content of the host olivine, then it may be possible to discount the role of diffusion in generation of the poor correlation between Fo and $\delta^{18}O_{ol}$.

[52] An alternative explanation for the apparent inconsistency between the olivine and clinopyroxene Mg#-$\delta^{18}O$ data is that it may arise from differences in the quantity and quality of data available for the different minerals. In contrast to the olivine data, the clinopyroxene measurements were almost all taken from composite samples, and the correlations are based on 6–8 rather than 15–20 points. The chances of producing spurious correlations increases with decreasing number of points [*Sohn and Menke*, 2002; *Press et al.*, 1992]. For example, the null hypothesis of no correlation is accepted at the 0.05 significance level for both Mg# or La/Yb with clinopyroxene $\delta^{18}O$. The correlations observed for the olivine data are more robust than those for the clinopyroxenes, and interpretation of the poor correlation between the forsterite content of and the $\delta^{18}O$ of olivines leads to different conclusions to those based on the clinopyroxene data. In order to resolve this apparent conflict between the olivine and clinopyroxene data it will be necessary to acquire more $\delta^{18}O$ data, particularly from individual clinopyroxene crystals.

[53] The large variability in oxygen $\delta^{18}O$ that is present in Fo_{88-90} olivines mirrors the extreme melt inclusion REE variability, and may indicate that the origin of the $\delta^{18}O$ variation is same as that

of the REEs. The relationship between olivine forsterite content, $\delta^{18}O$ and melt inclusion La/Yb or La content is shown in Figure 16. While the highest $\delta^{18}O$ is found in two olivines with Fo_{91} and Fo_{89} that both contain melt inclusions with La/Yb < 0.4, the lowest $\delta^{18}O$ is found in olivines of Fo_{89-90} that contain melt inclusions with La/Yb > 1.3. These relationships indicate that the low $\delta^{18}O$ signal in the Borgarhraun olivines is associated with melts that have high Mg#s, similar to those of mantle melts, and high La/Yb. Such melts are unlikely to be produced by crustal processes (but see discussion in section 6.2), and are quite different to the low Mg# crustal assimilants proposed by *Nicholson et al.* [1991] or *Eiler et al.* [2000]. Further evidence in favor of a mantle origin for the lowest $\delta^{18}O$ Borgarhraun olivines can be found in Figure 16b. The low $\delta^{18}O$ olivines lie on a trend of increasing melt inclusion La content at near fixed forsterite content. However, olivine/melt inclusion pairs which lie on the differentiation trend of increasing La with decreasing forsterite content have intermediate $\delta^{18}O_{ol}$, indicating that modest amounts of crystallization are not linked to extreme variation in $\delta^{18}O$. This olivine/melt inclusion compositional trend can be accounted for by the AFC model of *Eiler et al.* [2000]. However, this AFC model does not predict $\delta^{18}O_{ol}$ of 3.3 per. mil. in the range of Theistareykir compositions, and the lowest $\delta^{18}O_{ol}$ predicted by the model is 4.2 per. mil. for melts in equilibrium with Fo_{83} olivines and with La contents of >2.5 ppm. Therefore the AFC model of *Eiler et al.* [2000] cannot account for the Fo_{90} olivines with low $\delta^{18}O$. The possible role of variable mantle melt compositions and assimilation processes in generating the observed variation in oxygen isotope ratios are further discussed below.

6. Discussion

6.1. A Mantle Origin for Oxygen Isotope Variability

[54] The relationships between $\delta^{18}O_{ol}$, crystal and melt inclusion compositions outlined above show that the low $\delta^{18}O$ signal in Borgarhraun olivines is associated with melts that have high Mg# and high
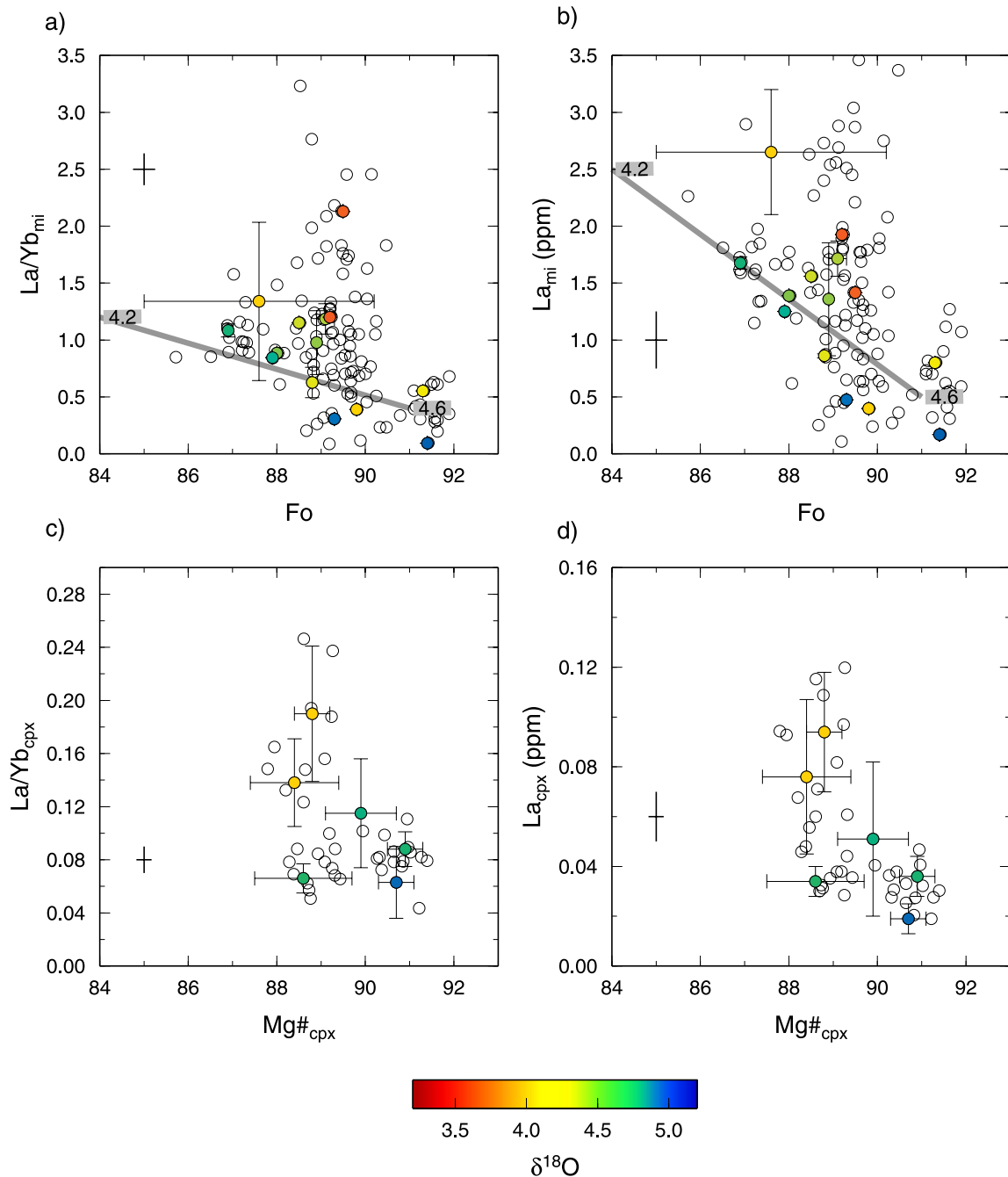
Figure 16. Relationship between REE and major element content and $\delta^{18}O$ of olivines, clinopyroxenes and melt inclusions. Figures 16a and 16b show the same data as Figure 8, with the addition of a number of colored points showing the $\delta^{18}O$ of the host olivine. The color scale for $\delta^{18}O$ is given at the base of the figure. The error bars on the colored points show the variability within single crystals or nodules (for composite samples). The cross without a circle shows the 1σ analytical precision. The AFC trend proposed by *Eiler et al.* [2000] is shown as a thick grey line. This line is best fit to the Theistareykir whole-rock sample data from *Eiler et al.* [2000], with melt Mg#s converted into equilibrium olivine forsterite contents using a K_d^{Fe-Mg} of 0.3 and Fe^{2+}/Fe^{tot} of 0.9. The numbers on the grey boxes show the variation in $\delta^{18}O_{ol}$ associated with this trend.

La/Sm. This association can be accounted for if mantle melts being supplied to Theistareykir are variable in $\delta^{18}O$, just as they are in trace element contents [*Slater et al.*, 2001; *Maclennan et al.*, 2002] and radiogenic isotope ratios [*Stracke et al.*, 2003]. The total range of $\delta^{18}O_{ol}$ is at least 3.3–5.2 per. mil., and may be even greater. There is a strong correlation between the La contents of Theistareykir basalts and picrites and their radiogenic isotope composition [*Stracke et al.*, 2003] and this correlation may be due to the presence of variable quantities of ancient recycled oceanic basalt within the Theistareykir mantle source. The $\delta^{18}O$ of oceanic crust is typically greater than 3.5 per. mil. [*Gregory and Taylor*, 1981; *Muehlenbachs*, 1986], so it is not likely that addition of such material to standard mantle peridotite, which has a $\delta^{18}O$ of ~5.5 per. mil. [*Mattey et al.*, 1994], can account for the lowest $\delta^{18}O$ values in Borgarhraun olivines. However, $\delta^{18}O$ of as low as 2 per. mil. have been reported from mantle eclogites found as xenoliths in kimberlites [*Lowry et al.*, 1999; *Eiler*, 2001] and the melting of such material in the mantle under Theistareykir may be able to account for the oxygen isotope compositions of the Borgarhraun olivines. *McKenzie and Stracke* [2002] have suggested that the correlation between trace element concentrations and radiogenic isotopes may be caused by addition of recycled ocean island basalt (OIB) to a depleted mantle source. If this OIB interacted with low $\delta^{18}O$ meteoric water before being recycled, then melting of this enriched source may produce melts with high La/Yb and low enough $\delta^{18}O$ to match the Borgarhraun olivine values. Unfortunately, it is not yet possible to investigate the relationship between $\delta^{18}O$ and radiogenic isotopes, because radiogenic isotope measurements are not yet available from the Theistareykir crystals or melt inclusions.

6.2. Alternative Mechanisms for Generating the Variation in REE Concentrations and Oxygen Isotopes

[55] While fractional melting of a heterogeneous mantle source followed by concurrent mixing and crystallization can account for the observed geochemical variations in the Borgarhraun melt inclusions and their host olivines, a number of other processes are also capable of generating geochemical variability in Icelandic magma. The ability of AFC processes to account for the variation in evolved lava from Krafla and Theistareykir has been demonstrated by *Nicholson et al.* [1991] and *Eiler et al.* [2000]. However, these AFC models predict that increases in REE concentrations and decreases in $\delta^{18}O$ should be associated with decreasing Mg# of melt. Therefore such mechanisms alone are not able to account for the variations observed in melt inclusion REE contents and $\delta^{18}O$ in forsteritic olivines from Borgarhraun. As discussed in section 5.3, Mg-Fe diffusion in olivine is rapid, and may reset the forsterite content of olivines within a few hundred years. However, variable assimilation of a low Mg#, low $\delta^{18}O$, high REE content material, followed by diffusional equilibration in high Mg# melts, which provides forsteritic host olivines, cannot reproduce the Borgarhraun observations. One reason for this failure is that the compositional trends for the melt inclusions are different to those for the whole rock samples, and *Eiler et al.* [2000] emphasized this point using the La/Sm versus CaO/Na_2O systematics of the melt inclusions and whole rock samples. Another weakness of the AFC-diffusion proposal is that it does not account for the observed decrease in La/Yb variation of the melt inclusions with decreasing forsterite content of the host olivine, because some low forsterite olivines would be expected to contain melt inclusions with high La/Yb.

[56] However, it is not possible to rule out all assimilation and crystallization processes as the cause of the observed REE or oxygen isotope variability. For instance, assimilation of a solidified gabbro with the composition of basalt from the Gaesafjöll eruption, which is located about 5 km to the south of the Borgarhraun vent, may be able to account for the REE variability. This eruption has an average La content of ~7 ppm, a La/Yb ratio of ~3.5 and a relatively high Mg# which is in equilibrium with Fo_{86} olivines. If such magma solidified near the Moho and was altered by hydrothermal fluids then a low $\delta^{18}O$ gabbro with high REE contents could be produced. Wholesale assimilation and melting of this gabbro in a depleted mantle melt may be able to generate

the variability observed in melt inclusion REE contents. This variability could then by diminished during mixing and crystallization, as described previously. One important point about this assimilation model is that the REE variation still has its origins in the mantle, and any correlation between REE enrichment in the assimilant and low $\delta^{18}O$ is coincidental. *Maclennan et al.* [2002] demonstrated that the composition of Gaesafjöll cannot be related to those of low La/Yb eruptions like Borgarhraun through magma chamber processes such as in situ crystallization [*Langmuir*, 1989] or steady-state replenished-tapped-fractionated crystallization [*O'Hara and Mathews*, 1981] unless garnet or other phases that can cause extreme fractionation of light, middle and heavy REEs are present. Similar arguments can be applied to the REE variation observed for the melt inclusions because it is not possible to simultaneously match the variations in REE concentrations and REE/Yb ratios with modest variations in compatible element concentrations (<50%) unless garnet or a phase with similar partition coefficients is present in the magma chambers. In order for garnet to be present during crystallization of basalts with compositions similar to those of Borgarhraun pressures of 1.5 GPa are required [*Bernstein*, 1994], higher than those estimated for crystallization of Borgarhraun. Therefore it seems likely that the REE variability reflects variation in the composition of mantle melts, as does the variation in long-lived isotopic variation found in whole-rock samples from Theistareykir [*Stracke et al.*, 2003]. While we cannot rule out crustal assimilation as the cause of the variation in oxygen isotopes in the olivines, the variation in $\delta^{18}O$ found in Fo$_{\sim90}$ olivines indicates that the REE variation in melt inclusions and the $\delta^{18}O$ in their host olivines may have a common origin in the mantle.

6.3. Melt Inclusion Variability and Spatial Variability

[57] The spatial distribution of moderately incompatible elements (e.g., Yb) in Borgarhraun is strongly non-random on the scale of kilometres, so that samples separated by less than 4 km have more similar concentrations of moderately incompatible elements than those expected from a ran-

dom distribution of compositions within the flow [*Maclennan et al.*, 2003]. This spatial distribution may be produced by mixing of batches of melt in a magma body before episodic extraction of melt from that body and eruption. The present-day separation of samples is controlled in part by deformation during flow as lava on the surface so that rocks separated by large distances may have been more closely spaced as melt in magma chambers. In contrast to the moderately incompatible elements a number of highly incompatible elements, such as La, have spatial distributions that are close to random at all length scales that could be resolved by the sampling of *Maclennan et al.* [2003]. This difference in the strength of non-random spatial distribution between La and Yb cannot be accounted for by the simple mixing process proposed by *Maclennan et al.* [2003], because this mixing should mix all of the elements over the same length scales. La and Yb also display differences in mixing behavior on plots such as those shown in Figure 13. It is possible that these differences in mixing history and spatial distribution of La and Yb are generated by the addition of deep melts produced during the initial stages of melting to a mixing magma chamber. Such melts have high La, low Yb and low Mg#, will generate La variability in melts that have similar Mg#s to the Borgarhraun whole rock samples and are in equilibrium with olivines with forsterite contents between 88 and 90 mol% (Figure 6). However, these melts have Yb contents close to the mean predicted melt composition and will not generate Yb variability. The sampling of *Maclennan et al.* [2003] was not able to resolve non-random elemental distributions at sample separations of less than 2 km due to the limited sampling density of the flow. If these initial melts were introduced to the magma body at a length scale smaller than that which can be resolved by the Borgarhraun whole-rock sampling, the apparent La distribution would be close to random at sample separations of >2 km. Since the initial melts do not have extreme Yb concentrations, their addition to the mixing magma chamber will not have a strong influence of the length scale of variability for Yb. If such processes took place in the melt bodies that supplied Borgarhraun, then fine-scale sampling of whole rock samples from a

small part of the flow should exhibit non-random variation in highly incompatible elements.

6.4. Convection in Lower Crustal Magma Bodies

[58] The decrease in the forsterite content of olivines and the increase in the average REE concentration in melt inclusions are caused by cooling and crystallization of basaltic melt. The decrease in compositional variability in melt inclusion compositions can be generated by mixing of melt. The Borgarhraun observations indicate that crystallization, cooling and mixing of melt are coupled processes with greater degrees of mixing as cooling proceeds. This coupling is expected if cooling in the magma chamber takes place by convection. In laboratory experiments designed as analogues to magma chambers the cooling rate is controlled by the Rayleigh number of the convection [e.g., *Jaupart and Brandeis*, 1986]. Convection within the melt will also cause stirring [*Eckart*, 1948], so that compositional heterogeneities will be stretched and thinned. As stirring progresses, diffusion in the liquid will result in mixing (sensu stricto) and compositional variation within the liquid will decrease. Experimental studies have shown that the thermodynamic mixing efficiency in magma chambers is related to the Reynolds number of the flow [*Jellinek and Kerr*, 1999], but have neither been able to link thermodynamic mixing to compositional mixing nor to quantify the rate of mixing within the experiments. Therefore although the relative rates of mixing and cooling that have been estimated from the Borgarhraun observations have the potential to provide useful constraints on the physics of magma chambers, further description of the theory of compositional mixing as applied to magma chambers is required before the observations can be used to constrain magma chamber properties.

6.5. Melting, Mixing, Crystallization and Eruption

[59] The observations presented in this work can be used to refine the synthesis of the evolution of the Borgarhraun melt given by *Maclennan et al.* [2003]. Fractional melting of mantle with a variable source composition generates melts with a large compositional range [*Slater et al.*, 2001; *Stracke et al.*, 2003]. These melts rise toward the surface at average velocities of at least 50 m yr^{-1} [*Maclennan et al.*, 2002]. Since the range of observed melt inclusion compositions is greater than that predicted by fractional melting models of a single source, it is likely that some mixing takes place before the onset of crystallization, perhaps in high porosity channels that form conduits for the rising melt [*Kelemen et al.*, 1997]. As the melts approach the surface they start to cool and crystallization commences at pressures of $\sim$0.9 GPa. This pressure corresponds to a depth of $\sim$30 km, which is greater than the crustal thickness of $\sim$21 km observed at Theistareykir [*Staples et al.*, 1997]. Crystallization may take place either within the channels or in magma bodies such as those thought to have generated gabbroic sills in the MTZ of the Oman ophiolite [*Boudier et al.*, 1996; *Korenaga and Kelemen*, 1997]. Convection in such sills causes concurrent cooling, stirring and mixing of the melt as recorded in the variation in melt inclusion and mineral compositions. It is likely that mantle melt is continuously being added to mixing magma bodies, so that the average temperature of the melt can increase as well as decrease with time. The non-random pattern of spatial variability observed in the moderately incompatible elements can be produced if the magma chamber episodically supplies melt to the surface in batches of about 0.01– 0.1 km^3 volume and these batches flow over the surface during eruptive events. Episodic fracturing of magma chamber walls is consistent both with field observations of fissure eruptions in northern Iceland and with simple physical models of magma bodies in the lower oceanic crust [*Kelemen and Aharonov*, 1998]. The extraction of melt from the magma chamber and its transport toward the surface in dykes may lead to further stirring and mixing and contribute to relative homogeneity in products of single eruptive events. If the average composition of melt being added to the body changes over time, then the composition of the products of each eruptive event will be slightly different, producing non-random spatial variability. This model of production of fractional melts from a heterogeneous source followed by incomplete

mixing and crystallization in near-Moho magma bodies can account for the Borgarhraun crystal and melt inclusion compositions. However, models where a single primary mantle melt undergoes closed-system fractional crystallization to produce a single liquid line of descent are not consistent with the observations. Such an approach has been widely used to model the composition of MORB samples, and the interpretation of the results of such models should be undertaken with caution until melt mixing is better understood.

7. Conclusions

[60] Crystals in Borgarhraun nodules show a similar range of compositions to those present as phenocrysts, and about 80% of these crystals are in Mg-Fe equilibrium with melts that have the composition of Borgarhraun whole rock samples. The average olivine-hosted melt inclusion REE composition is similar to that of the average whole-rock. The Borgarhraun nodules crystallized from a melt with a similar composition to that of Borgarhraun and may have crystallized from part of the same mixing melt body that provided the magma for the Borgarhraun eruptions.

[61] While the maximum average forsterite content of plagioclase-bearing nodules is $Fo_{88.5}$, clinopyroxene is found in nodules where the average forsterite content of the olivine is up to $Fo_{91.6}$. This observation indicates that plagioclase joined the crystallizing assemblage at greater extents of crystallization and lower temperatures than clinopyroxene. This behavior is expected when basalt crystallization takes place at pressures of >0.8 GPa, which corresponds to depths similar to or slightly greater than that of the Moho under Theistareykir. These crystallization pressure estimates are similar to the 0.8–0.9 GPa obtained from both clinopyroxene-melt equilibria and melt compositions of Borgarhraun whole-rock samples.

[62] The relationship between the variability of melt inclusion REE compositions and the forsterite content of their host olivine provides a record of concurrent mixing and crystallization of melt. The standard deviation of melt inclusion La concen-

trations hosted in Fo_{87} olivines is a factor of 4 lower than those hosted in Fo_{90} olivines and this reduction in variability is likely to result from melt mixing. The change in olivine compositions corresponds to a crystallization interval of ~20% or a reduction in temperature of 50–70°C. The relative rates of mixing (quantified with a parameter, M) and crystallization or cooling are $dM/dF \sim 2.5$ and $dM/dT \sim -8 \times 10^{-3}$ °C^{-1}. An increase in variability between Fo_{92} and Fo_{90} may reflect the establishment of geochemical variation by mantle melts generated at different depths and extents of melting. Introduction of mantle melts to the mixing and cooling magma body may be the cause for differences in the apparent mixing behaviour of La and Yb.

[63] Oxygen isotope variations in olivine crystals from Borgarhraun phenocrysts and nodules are highly variable, with $\delta^{18}O$ from 3.3 to 5.2 per mil. The full range of oxygen isotope variation is present in olivines with Fo_{89-90}, and the low $\delta^{18}O$ signal is associated with melts of high Mg# and La/Yb. Such geochemical relationships cannot be produced by assimilation of low Mg# crustal materials alone, and may reflect oxygen isotopic variation within the mantle source.

[64] The compositions of crystals and melt inclusions hosted by Borgarhraun samples can be accounted for by fractional melting of a heterogeneous mantle source followed by concurrent mixing and crystallization at Moho depths or deeper. The observations are not consistent with closed system low pressure fractional crystallization of a single primary mantle melt composition.

Acknowledgments

References

Albarède, F., *Introduction to Geochemical Modeling*, Cambridge Univ. Press, New York, 1995.

Baker, M. B., and E. M. Stolper, Determining the composition of high-pressure mantle melts using diamond aggregates, *Geochim. Cosmochi. Acta*, *58*, 2811–2827, 1994.

Baker, M. B., M. M. Hirschmann, M. S. Ghiorso, and E. M. Stolper, Compositions of near-solidus peridotite melts from experiments and thermodynamic calculations, *Nature*, *375*, 308–311, 1995.

Beattie, P., Olivine-melt and orthopyroxene-melt equilibria, *Contrib. Mineral. Petrol.*, *115*, 103–111, 1993.

Bender, J. F., F. N. Hodges, and A. E. Bence, Petrogenesis of basalts from the project FAMOUS area: Experimental study from 0 to 15 kbars, *Earth Planet. Sci. Lett.*, *41*, 277–302, 1978.

Bernstein, S., High-pressure fractionation in rift-related basaltic magmatism: Faeroe plateau basalts, *Geology*, *22*, 815–818, 1994.

Boudier, F., A. Nicolas, and B. Ildefonse, Magma chambers in the Oman ophiolite: Fed from the top and the bottom, *Earth Planet. Sci. Lett.*, *144*, 239–250, 1996.

Chakraborty, S., Rates and mechanisms of Fe-Mg interdiffusion in olivine at $980°–1300°C$, *J. Geophys. Res.*, *102*, 12,317–12,331, 1997.

Chiba, H., T. Chacko, R. N. Clayton, and J. R. Goldsmith, Oxygen isotope fractionations involving diopside, forsterite, magnetite, and calcite: Application to geothermometry, *Geochim. Cosmochim. Acta*, *53*, 2985–2993, 1989.

Danyushevsky, L. V., The effect of small amounts of H_2O on crystallization of mid-ocean ridge and backarc basin magmas, *J. Volcanol. Geotherm. Res.*, *110*, 265–280, 2001.

Dimanov, A., and V. Sautter, "Average" interdiffusion of (Fe,Mn)-Mg in natural diopside, *Eur. J. Min.*, *12*, 749–760, 2000.

Dimanov, A., O. Jaoul, and V. Sautter, Calcium self-diffusion in natural diopside single crystals, *Geochim. Cosmochim. Acta*, *60*, 4095–4106, 1996.

Eckart, C., An analysis of stirring and mixing processes in incompressible fluids, *J. Mar. Res.*, *7*, 265–275, 1948.

Eiler, J. M., Oxygen isotope variations of basaltic lavas and upper mantle rocks, *Rev. Mineral. Geochem.*, *43*, 319–364, 2001.

Eiler, J. M., K. Grönvold, and N. Kitchen, Oxygen isotope evidence for the origin of chemical variation in the lavas of Theistareykir volcano in Iceland's Northern Volcanic Zone, *Earth Planet. Sci. Lett.*, *184*, 269–286, 2000.

Elliott, T. R., C. J. Hawkesworth, and K. Grönvold, Dynamic melting of the Iceland plume, *Nature*, *351*, 201–206, 1991.

Ford, C. E., D. G. Russell, J. A. Craven, and M. R. Fisk, Olivine liquid equilibria - temperature, pressure and composition dependence of the crystal liquid cation partition coefficients for Mg, Fe^{2+}, Ca and Mn, *J. Petrol.*, *24*, 256–265, 1983.

Gaetani, G. A., and E. B. Watson, Open system behavior of olivine-hosted melt inclusions, *Earth Planet. Sci. Lett.*, *183*, 27–41, 2000.

Gautason, B., and K. Muehlenbachs, Oxygen isotopic fluxes associated with high temperature processes in the Rift Zones of Iceland, *Chem. Geol.*, *145*, 275–286, 1998.

Gregory, R. T., and H. P. Taylor, An oxygen isotope profile in a section of cretaceous oceanic crust, Samail Ophiolite, Oman: Evidence for $\delta^{18}O$ Buffering of the oceans be deep (>5 km) seawater-hydrothermal circulation at mid-ocean ridges, *J. Geophys. Res.*, *86*, 2737–2755, 1981.

Grove, T. L., M. B. Baker, and R. J. Kinzler, Coupled CaAl-NaSi diffusion in plagioclase feldspar: Experiments and applications to cooling rate speedometry, *Geochim. Cosmochim. Acta*, *48*, 2113–2121, 1984.

Gurenko, A. A., and M. Chaussidon, Oxygen isotope variations in primitive tholeiites of Iceland: Evidence from a SIMS study of glass inclusions, olivine phenocrysts and pillow rim glasses, *Earth Planet. Sci. Lett.*, *205*, 63–79, 2002.

Hémond, C., N. T. Arndt, U. Lichtenstein, and A. W. Hofmann, The Heterogeneous Iceland Plume: Nd-Sr-O isotopes and Trace element constraints, *J. Geophys. Res.*, *98*, 15,833–15,850, 1993.

Hirschmann, M. M., M. B. Baker, and E. M. Stolper, The effect of alkalis on the silica content of mantle-derived melts, *Geochim. Cosmochim. Acta*, *62*, 883–902, 1998.

Hirschmann, M. M., M. S. Ghiorso, and E. M. Stolper, Calculation of peridotite partial melting from thermodynamic models of minerals and melts: II. Isobaric variations in melts near the solidus and owing to variable source composition, *J. Petrol.*, *40*, 297–313, 1999.

Ito, M., H. Yurimoto, M. Morioka, and H. Nagasawa, Co2+ and Ni2+ diffusion in olivine determined by secondary ion mass spectrometry, *Phys. Chem. Miner.*, *26*, 425–431, 1999.

Jaupart, C., and G. Brandeis, The stagnant bottom layer of convecting magma chambers, *Earth Planet. Sci. Lett.*, *80*, 183–199, 1986.

Jellinek, A. M., and R. C. Kerr, Mixing and compositional stratification produced by natural convection: 2. Applications to the differentiation of basaltic and silicic magma chambers and komatiite lava flows, *J. Geophys. Res.*, *104*, 7203–7218, 1999.

Johnson, K. T. M., H. J. B. Dick, and N. Shimizu, Melting in the oceanic upper mantle: An ion microprobe study of diopsides in abyssal peridotites, *J. Geophys. Res.*, *95*, 2661–2678, 1990.

Jurewicz, A. J. G., and E. B. Watson, Cations in olivine: 2. Diffusion in olivine xenocrysts, with applications to petrology and mineral physics, *Contrib. Mineral. Petrol.*, *99*, 186–201, 1988.

Kelemen, P. B., and E. Aharonov, Periodic formation of magma fractures and generation of layered gabbros in the lower crust beneath oceanic spreading ridges, in *Faulting and Magmatism at Mid-ocean Ridges*, *Geophys. Monogr. Ser.*, vol. 106, edited by R. W. Buck et al., pp. 267–289, AGU, Washington, D.C., 1998.

Kelemen, P. B., G. Hirth, N. Shimizu, M. Spiegelman, and H. J. B. Dick, A review of melt migration processes in the asthenospheric mantle beneath oceanic spreading centers,

Philos. Trans. R. Soc. London Ser. A, 355, 283–318, 1997.

Kilinc, A., I. S. E. Carmichael, M. L. Rivers, and R. O. Sack, The ferric-ferrous ratio of natural silicate liquids equilibrated in air, *Contrib. Mineral. Petrol., 83*, 136–140, 1983.

Koga, K. T., P. B. Kelemen, and N. Shimizu, Petrogenesis of the crust-mantle transition zone and the origin of lower crustal wehrlite in the Oman ophiolite, *Geochem. Geophys. Geosyst., 2*, Paper number 2000GC000132, 2001.

Kogiso, T., K. Hirose, and E. Takahashi, Melting experiments on homogeneous mixtures of peridotite and basalt: Application to the genesis of ocean island basalts, *Earth Planet. Sci. Lett., 162*, 45–61, 1998.

Kohler, T. P., and G. P. Brey, Calcium exchange between olivine and clinopyroxene calibrated as a geothermobarometer for natural peridotites from 2 to 60 kb, *Geochim. Cosmochim. Acta, 54*, 2375–2388, 1990.

Korenaga, J., and P. B. Kelemen, Origin of gabbro sills in the Moho transition zone of the Oman ophiolite: Implications for magma transport in the oceanic lower crust, *J. Geophys. Res., 102*, 27,729–27,749, 1997.

Langmuir, C. H., Geochemical consequences of in situ crystallization, *Nature, 340*, 199–205, 1989.

Longhi, J., Some phase equilibrium systematics of lherzolite melting: I, *Geochem. Geophys. Geosyst., 3*(3), 1020, doi:10.1029/2001GC000204, 2002.

Loucks, R. R., A precise olivine-augite Mg-Fe exchange geothermometer, *Contrib. Mineral. Petrol., 125*, 140–150, 1996.

Lowry, D., D. P. Mattey, and J. W. Harris, Oxygen isotope composition of syngenetic inclusions in diamond from the Finsch Mine, RSA, *Geochim. Cosmochim. Acta, 63*, 1825–1836, 1999.

Maclennan, J., D. McKenzie, K. Grönvold, and L. Slater, Crustal accretion under northern Iceland, *Earth Planet. Sci. Lett., 191*, 295–310, 2001a.

Maclennan, J., D. McKenzie, and K. Grönvold, Crustal accretion under northern Iceland, *Earth Planet. Sci. Lett., 194*, 67–82, 2001b.

Maclennan, J., M. Jull, D. McKenzie, L. Slater, and K. Grönvold, The link between volcanism and deglaciation in Iceland, *Geochem. Geophys. Geosyst., 3*(11), 1062, doi:10.1029/2001GC000282, 2002.

Maclennan, J., D. McKenzie, F. Hilton, K. Gronvld, and N. Shimizu, Geochemical variability in a single flow from northern Iceland, *J. Geophys. Res., 108*(B1), 2007, doi:10.1029/2000JB000142, 2003.

Mattey, D. P., D. Lowry, and C. G. Macpherson, Oxygen isotope composition of mantle peridotite, *Earth Planet. Sci. Lett., 128*, 231–241, 1994.

McKenzie, D., and R. K. O'Nions, Partial melt distributions from inversion of rare earth element concentrations, *J. Petrol., 32*, 1021–1091, 1991.

McKenzie, D., and A. Stracke, The association of heat and isotopes beneath Iceland, paper presented at the Superplume Workshop Tokyo 2002, Tokyo Institute of Technology, Tokyo, 2002.

Muehlenbachs, K., Alteration of the oceanic crust and the $\delta^{18}O$ history of seawater, *Rev. Mineral., 16*, 425–444, 1986.

Nicholson, H., M. Condomines, J. G. Fitton, A. E. Fallick, K. Grönvold, and G. Rogers, Geochemical and Isotopic Evidence for Crustal Assimilation Beneath Krafla, Iceland, *J. Petrol., 32*, 1005–1020, 1991.

O'Hara, M. J., and R. E. Mathews, Geochemical evolution in an advancing, periodically replenished, periodically tapped, continuously fractionated magma chamber, *J. Geol. Soc. London, 138*, 237–277, 1981.

Press, W. H., B. P. Flannery, S. A. Teukolsky, and W. T. Vetterling, *Numerical Recipes*, Cambridge Univ. Press, New York, 1992.

Putirka, K., Clinopyroxene plus liquid equilibria to 100 kbar and 2450 K, *Contrib. Mineral. Petrol., 135*, 151–163, 1999.

Putirka, K., M. Johnson, R. Kinzler, J. Longhi, and D. Walker, Thermobarometry of mafic igneous rocks based on clinopyroxene-liquid equilibria, 0–30 kbar, *Contrib. Mineral. Petrol., 123*, 92–108, 1996.

Reed, S. J. B., *Electron Microprobe Analysis and Scanning Electron Microscopy in Geology*, Cambridge Univ. Press, New York, 1996.

Robinson, J. A. C., B. J. Wood, and J. D. Blundy, The beginning of melting of fertile and depleted peridotite at 1.5 GPa, *Earth Planet. Sci. Lett., 155*, 97–111, 1998.

Roeder, P. L., and R. F. Emslie, Olivine-liquid equilibrium, *Contrib. Mineral. Petrol., 29*, 275–289, 1970.

Shimizu, N., The geochemistry of olivine-hosted melt inclusions in a FAMOUS basalt ALV519-4-1, *Phys. Earth Planet. Inter., 107*, 183–201, 1998.

Shimizu, N., and S. R. Hart, Applications of the ion microprobe to geochemistry and cosmochemistry, *Ann. Rev. Earth. Planet. Sci., 10*, 483–526, 1982.

Sigurdsson, I. A., S. Steinthorsson, and K. Grönvold, Calcium-rich melt inclusions in Cr-spinels from Borgarhraun, northern Iceland, *Earth Planet. Sci. Lett., 183*, 15–26, 2000.

Skovgaard, A. C., M. Storey, J. Baker, J. Blusztajn, and S. R. Hart, Osmium-oxygen isotopic evidence for a recycled and strongly depleted component in the Iceland mantle plume, *Earth Planet. Sci. Lett., 194*, 259–275, 2001.

Slater, L., Melt generation beneath Iceland, Ph.D. Thesis, Univ. of Cambridge, Cambridge, 1996.

Slater, L., D. McKenzie, K. Grönvold, and N. Shimizu, Melt generation and movement beneath Theistareykir, N.E. Iceland, *J. Petrol., 42*, 321–354, 2001.

Sohn, R. A., and W. Menke, Application of maximum likelihood and bootstrap methods to nonlinear curve-fit problems in geochemistry, *Geochem. Geophys. Geosyst., 3*(7), 1041, doi:10.1029/2001GC000253, 2002.

Staples, R. K., R. S. White, B. Brandsdóttir, W. Menke, P. K. H. Maguire, and J. H. McBride, Färoe-Iceland Ridge Experiment 1. Crustal structure of northeastern Iceland, *J. Geophys. Res., 102*, 7849–7866, 1997.

Stracke, A., A. Zindler, V. J. M. Salters, D. McKenzie, J. Blichert-Toft, F. Albarède, and K. Grönvold, Theistareykir revisited, *Geochem. Geophys. Geosyst.*, *4*(2), 8507, doi:10.1029/2001GC000201, 2003.

Sveinbjörnsdóttir, A. E., M. L. Coleman, and B. W. D. Yardley, Origin and history of hydrothermal fluids of the Reykjanes and Krafla geothermal fields, Iceland: A stable isotope study, *Contrib. Mineral. Petrol.*, *94*, 99–109, 1986.

Van Orman, J. A., T. L. Grove, and N. Shimizu, Rare earth element diffusion in diopside: Influence of temperature, pressure, and ionic radius, and an elastic model for diffusion in silicates, *Contrib. Mineral. Petrol.*, *141*, 687–703, 2001.

Watson, S., and D. McKenzie, Melt generation by plumes: A study of Hawaiian volcanism, *J. Petrol.*, *32*, 501–537, 1991.

Weaver, J. S., and C. H. Langmuir, Calculation of phase-equilibrium in mineral melt systems, *Comput. Geosci.*, *16*, 1–19, 1990.

Wood, B. J., and J. D. Blundy, A predictive model for rare earth element partitioning between clinopyroxene and anhydrous silicate melt, *Contrib. Mineral. Petrol.*, *129*, 166–181, 1997.